J. Mech. Phys. Solids 215 (2026) 106732

Contents lists available at ScienceDirect

Journal of the Mechanics and Physics of Solids

journal homepage: www.elsevier.com/locate/jmps

A unified duality theory between self-stress and folding mechanisms

Xiangxin Dang [a], Glaucio H. Paulino [a,b,*]

[a] Department of Civil and Environmental Engineering, Princeton University, Princeton, NJ, 08544, USA
[b] Princeton Materials Institute (PMI), Princeton University, Princeton, NJ, 08544, USA

ARTICLE INFO

Keywords:
Duality
Tensegrity
Origami
Maxwell's rule
Cauchy's rigidity theorem

ABSTRACT

The generalized Maxwell's rule, a central result in structural mechanics, reveals the combinatorial relationship between the states of self-stress and the infinitesimal mechanisms of a pin-jointed framework. In particular, when the framework forms the skeleton of a polyhedron that is closed and homeomorphic to a sphere, the number of independent states of self-stress equals the number of independent infinitesimal mechanisms. In this paper, we establish an analytical formulation of this equivalence, manifested through the dual relationship of stable tensegrity and shaky origami. The infinitesimal folding mechanisms of the origami are expressed in terms of nodal displacements and subsequently projected onto dihedral-angle variations, which are shown to be dual to the self-stress of the corresponding tensegrity. This duality extends Cauchy's rigidity theorem from convex polyhedra, where both self-stress and folding mechanisms vanish, to nonconvex polyhedra, where nonzero but equivalent states of self-stress and folding mechanisms coexist. The duality theory can be potentially used to construct shaky origami structures based on known tensegrity configurations, and conversely, to generate self-stressed tensegrity systems from existing origami designs.

1. Introduction

This paper establishes a fundamental theory for characterizing the duality between self-stress and folding mechanisms in polyhedral pin-jointed frameworks. We formulate origami folding mechanisms in terms of nodal displacements and subsequently projecting these displacements onto dihedral-angle variations. The folding mechanisms are then shown to be dual to the states of self-stress of the corresponding tensegrity. *This formulation relies on matrix-based structural mechanics, which is readily amenable to programmatic implementation to identify dual stress and folding modes, and to compute the corresponding internal forces and nodal displacements*. In the remainder of this section, we provide a discussion on rigidity theory and duality principles, which form the basis for this work. In subsequent sections, we first develop the duality formulation based on triangulated polyhedra. Then, we introduce auxiliary members whose internal forces or folding angles are constrained to zero, thereby extending the formulation to tensegrity and origami configurations with general polygonal faces. We present a range of dual configurations, including spherical and tower-like forms. All the examples are associated with nonconvex polyhedra, as the convex ones do not admit infinitesimal flexibility, except in degenerate configurations with singular vertices surrounded by coplanar triangles.

* Corresponding author.
E-mail address: gpaulino@princeton.edu (G.H. Paulino).

https://doi.org/10.1016/j.jmps.2026.106732
Received 13 March 2026; Received in revised form 22 May 2026; Accepted 15 June 2026
Available online 17 June 2026

1.1. Rigidity theory of polyhedra

Rigidity theory predicts the rigidity or flexibility of structures based on their geometric constraints. A cornerstone therein is Cauchy's rigidity theorem, which infers that all convex polyhedra are rigid (Cauchy, 1813; Cromwell, 1997). Here, the polyhedra are composed of nondeformable faces hinged along their edges and *rigid* means the absence of any continuous deformation that preserves vertex distance within the faces and connectivity at the hinges, other than trivial rigid-body motions. The geometric feature of convexity is central in the further developments of polyhedron rigidity: strictly convex polyhedra are infinitesimally rigid (Dehn, 1916) and triangulated convex polyhedra are second-order rigid (Connelly, 1980). In this setting, infinitesimal (i.e., first-order) rigidity is defined as the property that no nontrivial deformation preserves the first-order derivatives of the vertex distances. Likewise, second-order rigidity means that any nontrivial deformation preserving the second-order derivatives of the vertex distances fails to preserve the first-order derivatives. Consequently, infinitesimal rigidity implies second-order rigidity, which in turn implies rigidity. In contrast to rigidity, flexibility arises in the presence of nonconvexity (Wells, 1997). Polyhedra that are infinitesimally flexible but not flexible—equivalently, rigid but not infinitesimally rigid—are referred to as *shaky polyhedra* (Goldberg, 1978). Canonical examples of shaky polyhedra include Blaschke's octahedron (Blaschke, 1920), Schönhardt's octahedron (Schönhardt, 1928), and Jessen's icosahedron (Jessen, 1967). All of them are nonconvex and composed of only triangular faces. The corresponding regular polyhedra, i.e., the icosahedron and the octahedron, are strictly convex and thus infinitesimally rigid. Beyond shakiness, the flexible polyhedra, which are continuously movable, are *extremely rare* (Gluck, 1975; Cromwell, 1997). Since Euler conjectured in 1766 that all polyhedra are rigid, it was not disproved until 1977, when Robert Connelly discovered the first flexible polyhedron (Connelly, 1976, 1977, 1979). This very first counterexample was constructed by adding "crinkled" dihedral surfaces to Bricard's 3D linkages (Bricard, 1897), yielding a flexible polyhedron with 30 faces (not all triangles), 50 edges, and 22 vertices (Demaine and O'Rourke, 2007a). The construction was later simplified by Nicolaas H. Kuiper and Pierre Deligne into a triangulated polyhedron with 11 vertices, 27 edges, and 18 faces and by Klaus Steffen into 9 vertices, 21 edges, and 14 faces (Connelly, 1978). Steffen's flexible polyhedron may be the simplest as it was proved that polyhedra with fewer than nine vertices are all rigid (Maksimov, 1995). The second simplest known triangulated flexible polyhedron, consisting of 10 vertices and 16 faces, was discovered by Tomohiro Tachi in 2011. It was later named the *two-tetrahedron flexible polyhedron* and reported by Li (2018). This polyhedron was used to significantly extend the rotation range of existing flexible polyhedra (from Steffen's 27° to Li's 80°) and to demonstrate that a single polyhedron can realize an arbitrary number of degrees of freedom (Li, 2018). In addition to infinitesimal and continuous deformations, nonconvex polyhedra may also admit multiple isolated configurations, as exemplified by the tristable Siamese dipyramids (Goldberg, 1978) and the bistable jumping octahedron (Wunderlich, 1986).

Historically, Cauchy's rigidity theorem was formulated in terms of the *congruence* of two polyhedra: *If two three-dimensional convex polyhedra P and P' are combinatorially equivalent with corresponding facets being congruent, then P is congruent to P'* (Aigner and Ziegler, 2010). The congruence of two polyhedra indicates the rigidity of a single one. That is, a convex polyhedron admits no alternative configurations, provided that the panels are not distorted or recombined. This physical rigidity can be formalized through the *skeletons* of polyhedra (Servatius, 2018). Interpreting a polyhedron as an assembly of rigid panels hinged along their edges naturally leads to the notion of the *2-skeleton*, defined as the collection of vertices, edges, and faces of the polyhedron. Under this interpretation, Cauchy's rigidity theorem establishes that the 2-skeleton of a convex polyhedron is rigid, thereby translating the mathematical notion of congruence into the physical notion of rigidity. In comparison, the *1-skeleton* of a polyhedron consists only of its vertices and edges and is naturally associated with a pin-jointed framework, in which vertices act as joints and edges as bars. However, unlike the hinged-panel model, even when the bars are rigid, the rigidity of a polyhedron is not always equivalent to the rigidity of its corresponding framework. This distinction is intuitive when comparing a cube composed of six rigid square panels with a cubic framework of twelve rigid bars. More precisely, the 1-skeleton of a strictly convex polyhedron is not rigid if it has at least one non-triangular face (Asimow and Roth, 1978). *As a consequence, triangulated polyhedra merit special attention, because their 1-skeletons and 2-skeletons—corresponding to the jointed bars and hinged panels, respectively—can be treated equivalently from the standpoint of rigidity.* Importantly, triangulating a convex polyhedron, in general, does not affect its rigidity. It was first proved by Alexandrov (1950) and further described by Asimow and Roth (1979) that if a strictly convex polyhedron is triangulated in such a way that no vertices are added in the interiors of faces, the resulting triangulated polyhedron is infinitesimally rigid. If the original strictly convex polyhedron contains any non-triangular faces, such a triangulation produces a polyhedron that is convex but not strictly convex. By dropping the requirement of *strict* convexity, Alexandrov's theorem implies that a triangulated, convex polyhedron is infinitesimally rigid, if it contains no vertex whose incident triangles all lie in a common plane. The remaining case is trivial: if all triangles incident to a vertex lie in a single plane, then lifting the interior vertex in the direction normal to that plane induces local infinitesimal rotations of the surrounding triangles, and hence the polyhedron is not infinitesimally rigid. As a result, nonconvexity is a necessary condition for the construction of flexible polyhedra, whether finitely or infinitesimally flexible, whose deformations occur globally.

1.2. Duality considerations

The concept of duality arises in pin-jointed frameworks through the presence of stress, defined as a set of real numbers, representing force densities assigned to each member of the framework. When this stress equilibrates forces at every node, the framework becomes a *tensegrity*. Mathematically, members of a tensegrity are classified as bars, struts, or cables (Demaine and O'Rourke, 2007b). Bars can sustain forces of arbitrary sign, struts can sustain only negative or zero forces, and cables can sustain only positive or zero forces. By contrast, from an engineering perspective, a tensegrity is typically considered to consist only of struts and cables (Skelton and De Oliveira, 2009; Zhang and Ohsaki, 2015; Gan, 2020; Fraternali and Rimoli, 2025). The rigidity or flexibility of a tensegrity

naturally extends that of a pin-jointed framework: rather than enforcing fixed member lengths in a flexible deformation (or *flex*, for short), struts are allowed to expand while cables are allowed to contract. In this setting, any infinitesimally rigid tensegrity (i.e., one that admits no nontrivial infinitesimal flex) must carry nonzero stress in all struts and cables (Roth and Whiteley, 1981). This result is termed the *first-order duality* by Connelly and Whiteley (1996), who reformulated it as the *first-order stress test*: a tensegrity has a first-order flex that strictly changes the length of a strut or cable if and only if every self-stress is zero on this member; and furthermore, they developed the *second-order stress test* by relating the second-order flex to the negative semi-definiteness of the stress matrix. These stress tests show that the equilibrium stress of a tensegrity is intertwined with its infinitesimal flex. This duality relationship is more explicit through the following equivalent statement of the first-order stress test (Demaine and O'Rourke, 2007b): *a tensegrity admits an equilibrium stress that is nonzero on a strut or cable if and only if every first-order flex preserves the length of that member.* Remarkably, both stress tests are universal and apply to tensegrities of arbitrary connectivity. As a result, such duality associates *one* flex with *all* stresses, or *one* stress with *all* flexes. This asymmetric correspondence, as articulated below, can be refined into a symmetric one when the tensegrity is a triangulated framework. Meanwhile, it is natural to align the triangulated framework with the concept of origami: a discrete foldable surface whose deformation is concentrated along creases (Misseroni et al., 2024). For example, when the surface is a triangulated polyhedron, the tensegrity corresponds to its 1-skeleton, whereas the origami corresponds to its 2-skeleton.

We elaborate the aforementioned symmetric correspondence between tensegrity and origami in the context of structural mechanics. A pin-jointed framework thereof is said to be statically indeterminate if it admits one or more states of self-stress, and kinematically indeterminate if it admits one or more infinitesimal mechanisms. The central result in indeterminacy analysis is the generalized Maxwell's counting rule (Maxwell, 1864; Pellegrino and Calladine, 1986), which associates the number of independent states of self-stress d_s and the number of infinitesimal mechanisms d_m to the number of members b and the number of nodes n, expressed as $d_s - (d_m + 6) = b - 3n$. Here, the states of self-stress are not zero-everywhere and the infinitesimal mechanisms are not rigid-body motions. That is, both are nontrivial. This formula can be further simplified if the framework is the 1-skeleton of a specific class of polyhedra, which are homeomorphic to a sphere and whose faces are triangles. The topological equivalence to a sphere leads to the Euler characteristic $\chi = n - b + f = 2$, with the face number f; and the triangulation indicates $3f = 2b$. Together, these relations give $b = 3n - 6$. In this case, the Maxwell's rule becomes $d_s = d_m$, indicating a one-to-one correspondence, i.e., the duality, between nontrivial states of self-stress and nontrivial infinitesimal mechanisms. A preliminary example of such a duality was reported by Tachi (2012), who showed that a shaky, triangulated origami tower forming a closed surface can be equivalently interpreted as a self-stressed prismatic tensegrity. This result is reminiscent of Connelly and Whiteley (1996)'s first-order duality (or first-order stress test) described above, but in a symmetric form. It suggests that the folding motions of flexible origami may be constructed from the balanced forces of self-stressed tensegrities, and vice versa.

Besides polyhedral configurations, the symmetric first-order duality has been used to analyze folding mechanisms of triangulated origami sheets that extend infinitely in space (McInerney et al., 2020). These periodic triangulated origami lie at the "Maxwell point," where the number of constraints equals the number of degrees of freedom. Specifically, this condition corresponds to $b = 3n$ for periodic pin-jointed frameworks, for which $\chi = 0$, rather than $b = 3n - 6$ for frameworks homeomorphic to a sphere, for which $\chi = 2$. Meanwhile, the imposed periodicity leads to the counting rule $d_s - (d_m + d_r) = b - 3n = 0$, whose interpretation *differs* from that for spherical frameworks (Guest and Hutchinson, 2003; McInerney et al., 2020). Here, d_m denotes the number of nontrivial infinitesimally flexible modes, and d_r the number of rigid-body modes compatible with the imposed periodicity. Spatially periodic sheets, such as Miura and eggbox origami, have $d_r = 3$, representing three independent translations but no rotations. In contrast, cylindrical sheets have $d_r = 2$, corresponding to one translational mode along the cylinder axis and one rotational mode about that axis. Moreover, d_s accounts not only for internal states of self-stress, but also for uniform tensile or shear stresses induced by loads applied at infinity in the periodic setting. Combining the periodic counting rule, $d_s = d_m + d_r$, and the force-folding duality, that each of the d_s self-stressed states pairs a linear folding mode, McInerney et al. (2020) showed that the two rigid-body modes ($d_r = 2$) of Maxwell cylindrical origami sheets imply two states of self-stress and, as a consequence of the duality, two folding modes. This analysis relies purely on the triangulation topology, rather than on the crease geometry, and elegantly corroborates the numerical results of Tachi (2015), who showed that triangular origami, including Resch's, waterbomb, and cylindrical Miura patterns, generally exhibit a two-dimensional space of folding configurations. Alongside the first-order duality, Connelly and Whiteley (1996)'s second-order duality (or second-order stress test) is significant for computing nonlinear folding motions of origami sheets. Following this, Chen and Santangelo (2018) derived a theory for distinguishing folding branches of developable origami near their unfolded state, which cannot be captured by linear folding motions.

In this paper, we focus on the first-order duality of infinitesimal mechanisms and states of self-stress associated with polyhedral frameworks, as we are interested in its symmetric form pertaining to finite structures. Tachi (2012)'s illustration of the triangulated origami tower and the prismatic tensegrity, obtained through numerical search for shaky origami, lacks a systematic theoretical development; however, it serves as an insightful example motivating our effort to establish such a theory. Also, we aim to generalize the triangulation-based theory to characterize the duality associated with polyhedra composed of general planar polygonal faces. Prior to Tachi (2012)'s illustration, Crapo and Whiteley (1982) had described the duality relationship defined on polygonal-panel polyhedra, as a contrapositive reformulation of the equivalence between static rigidity and infinitesimal rigidity. This establishment primarily involves the proof of existence of the duality from the perspective of projective geometry, and hence is not readily suited for quantitative structural analysis, such as determining the number of independent dual pairs, which we formulate in terms of the nullity of the equilibrium or kinematic matrices. Moreover, for both Crapo and Whiteley (1982)'s hinged polyhedra and Tachi (2012)'s shaky origami, the infinitesimal mechanisms are formulated in terms of dihedral-angle variations at hinges or creases. This setting is intuitive, as it reveals the duality relationship through an explicit correspondence between angular velocities and internal forces. That said, it is implicit for theoretical matrix analysis and computational implementation in structural mechanics.

While McInerney et al. (2020) provided one possible route by establishing a mapping from folding angles to nodal displacements in triangulated networks, nodal displacements are the variables directly associated with the kinematic matrix that describes the motion of pin-jointed frameworks. In our previous work (Dang and Paulino, 2026), we showed that, once the nodal displacements and dual internal forces are known for a given polyhedral framework, applying a nondegenerate linear transformation to the framework automatically determines the corresponding mechanism and equilibrium of the transformed framework. The new displacements, under the origami interpretation, and the new forces, under the tensegrity interpretation, can be explicitly calculated from the original ones through a linear formulation, while preserving the duality of tensegrity and origami, and even the super-stability of the tensegrity. In this way, starting from a single dual pair of tensegrity and origami, infinitely many such dual pairs can be directly generated, without the need for optimization or iterative computation. It is critical to identify an initial dual pair of tensegrity and origami as the seed for this optimization-free design process. This step would benefit from a systematic approach, rather than relying on an empirical choice (as in our previous work). Specifically, such an approach should determine whether the displacement and force modes exist simultaneously to support the duality, and, if so, how these modes can be calculated. Since the invariance theory (Dang and Paulino, 2026) preserves not only the duality but also the super-stability of tensegrities, we also discuss the super-stability of the tensegrities in the present work.

2. Preliminaries

We consider three-dimensional, free-standing, pin-jointed frameworks that are 1-skeletons of polyhedra. The frameworks, composed of free nodes and straight members, are interpreted as either tensegrities or linkages. In self-stressed tensegrities, the members are classified as struts or cables, whereas in flexible linkages they are rigid bars. Let b denote the number of members and n the number of nodes. We follow the notations in Zhang and Ohsaki (2015) to describe the geometry and connectivity of the frameworks. The vectors of nodal coordinates in the x, y, z directions are denoted by $\mathbf{x}$, $\mathbf{y}$, $\mathbf{z} \in \mathbb{R}^n$, respectively. The connectivity matrix $\mathbf{C} \in \mathbb{Z}^{b\times n}$ specifies how the nodes of a framework are linked by its members. The k-th row of $\mathbf{C}$ specifies the member k connecting node i and j, and its p-th entry is defined as

$$C_{k,p} = \begin{cases} \text{sign}(j-p), & \text{if} \quad p = i; \\ \text{sign}(i-p), & \text{if} \quad p = j; \\ 0, & \text{otherwise}, \end{cases} \tag{1}$$

where $k = 1, 2, \ldots, b$ and $p = 1, 2, \ldots, n$. Each entry $C_{k,p}$ thus takes a value in $\{+1, -1, 0\}$. Then, one can define the coordinate difference vectors $\mathbf{u}$, $\mathbf{v}$, $\mathbf{w} \in \mathbb{R}^b$ as

$$\mathbf{u} = \mathbf{C}\mathbf{x}, \ \mathbf{v} = \mathbf{C}\mathbf{y}, \ \mathbf{w} = \mathbf{C}\mathbf{z}, \tag{2}$$

respectively. We use $\mathbf{l} \in \mathbb{R}^b$ to denote the vector of member lengths. The k-th component ℓ_k, representing the length of member k, is expressed by

$$\ell_k = \sqrt{u_k^2 + v_k^2 + w_k^2}. \tag{3}$$

The diagonal matrices associated with $\mathbf{u}$, $\mathbf{v}$, $\mathbf{w}$, and $\mathbf{l}$ are defined as

$$\mathbf{U} = \text{diag}(\mathbf{u}), \quad \mathbf{V} = \text{diag}(\mathbf{v}), \quad \mathbf{W} = \text{diag}(\mathbf{w}), \quad \mathbf{L} = \text{diag}(\mathbf{l}), \tag{4}$$

respectively, where $\mathbf{U}$, $\mathbf{V}$, $\mathbf{W}$, $\mathbf{L} \in \mathbb{R}^{b\times b}$. Let $\mathbf{s} \in \mathbb{R}^b$ denote the member force vector, where the k-th component F_k represents the internal force in the member k. The equilibrium matrix $\mathbf{D} \in \mathbb{R}^{3n\times b}$ is given by

$$\mathbf{D} = \begin{bmatrix} \mathbf{C} & & \\ & \mathbf{C} & \\ & & \mathbf{C} \end{bmatrix}^{\mathrm{T}} \begin{bmatrix} \mathbf{U} \\ \mathbf{V} \\ \mathbf{W} \end{bmatrix} \mathbf{L}^{-1} = \begin{bmatrix} \mathbf{C}^{\mathrm{T}}\mathbf{U}\mathbf{L}^{-1} \\ \mathbf{C}^{\mathrm{T}}\mathbf{V}\mathbf{L}^{-1} \\ \mathbf{C}^{\mathrm{T}}\mathbf{W}\mathbf{L}^{-1} \end{bmatrix}. \tag{5}$$

Since no external forces are applied to free-standing frameworks, the equilibrium condition is

$$\mathbf{D}\mathbf{s} = \mathbf{0}. \tag{6}$$

We use $\mathbf{m} \in \mathbb{R}^{3n}$ to denote the infinitesimal mechanism vector. The p-th, $(p+n)$-th, and $(p+2n)$-th entries $\mathrm{d}x_p$, $\mathrm{d}y_p$, $\mathrm{d}z_p$ are the infinitesimal nodal displacements of the p-th node in the x, y, and z directions, respectively. The kinematic matrix $\mathbf{B} \in \mathbb{R}^{b\times 3n}$ is given by

$$\mathbf{B} = \mathbf{D}^{\mathrm{T}} = \begin{bmatrix} \mathbf{L}^{-1}\mathbf{U}\mathbf{C} & \mathbf{L}^{-1}\mathbf{V}\mathbf{C} & \mathbf{L}^{-1}\mathbf{W}\mathbf{C} \end{bmatrix}. \tag{7}$$

An infinitesimal mechanism does not change the member lengths, leading to the kinematic indeterminacy condition:

$$\mathbf{B}\mathbf{m} = \mathbf{0}. \tag{8}$$

The force density matrix $\mathbf{E}$ is useful for characterizing the equilibrium of pin-jointed frameworks. To provide its definition, we use $\mathbf{q} \in \mathbb{R}^b$ to denote the force density vector. The k-th component $q_k = F_k/\ell_k$ is the internal force density in the member k. In compact form, the force density vector can be written as

$$\mathbf{q} = \mathbf{L}^{-1}\mathbf{s}. \tag{9}$$

We further write the diagonal version of $\mathbf{q}$ as

$$\mathbf{Q} = \mathrm{diag}(\mathbf{q}). \tag{10}$$

The force density matrix $\mathbf{E} \in \mathbb{R}^{n\times n}$ is then defined by

$$\mathbf{E} = \mathbf{C}^{\mathrm{T}}\mathbf{Q}\mathbf{C}. \tag{11}$$

Using these definitions, we have

$$\mathbf{D}\mathbf{s} = \begin{bmatrix} \mathbf{C}^{\mathrm{T}}\mathbf{U}\mathbf{L}^{-1}\mathbf{s} \\ \mathbf{C}^{\mathrm{T}}\mathbf{V}\mathbf{L}^{-1}\mathbf{s} \\ \mathbf{C}^{\mathrm{T}}\mathbf{W}\mathbf{L}^{-1}\mathbf{s} \end{bmatrix} = \begin{bmatrix} \mathbf{C}^{\mathrm{T}}\mathbf{U}\mathbf{q} \\ \mathbf{C}^{\mathrm{T}}\mathbf{V}\mathbf{q} \\ \mathbf{C}^{\mathrm{T}}\mathbf{W}\mathbf{q} \end{bmatrix} = \begin{bmatrix} \mathbf{C}^{\mathrm{T}}\mathbf{Q}\mathbf{u} \\ \mathbf{C}^{\mathrm{T}}\mathbf{Q}\mathbf{v} \\ \mathbf{C}^{\mathrm{T}}\mathbf{Q}\mathbf{w} \end{bmatrix} = \begin{bmatrix} \mathbf{C}^{\mathrm{T}}\mathbf{Q}\mathbf{C}\mathbf{x} \\ \mathbf{C}^{\mathrm{T}}\mathbf{Q}\mathbf{C}\mathbf{y} \\ \mathbf{C}^{\mathrm{T}}\mathbf{Q}\mathbf{C}\mathbf{z} \end{bmatrix} = \begin{bmatrix} \mathbf{E}\mathbf{x} \\ \mathbf{E}\mathbf{y} \\ \mathbf{E}\mathbf{z} \end{bmatrix}. \tag{12}$$

Accordingly, the equilibrium condition Eq. (6) can be rewritten as

$$\mathbf{E}\mathbf{x} = \mathbf{0},\ \mathbf{E}\mathbf{y} = \mathbf{0},\ \mathbf{E}\mathbf{z} = \mathbf{0}. \tag{13}$$

Eq. (13) indicates that $\mathbf{x}$, $\mathbf{y}$, $\mathbf{z}$ are eigenvectors of $\mathbf{E}$ associated with the zero eigenvalue. Moreover, since a rigid translation of a tensegrity structure does not affect its self-equilibrium, the force density matrix $\mathbf{E}$ must admit an additional eigenvector $\mathbf{i}$, satisfying

$$\mathbf{E}\mathbf{i} = \mathbf{0}, \tag{14}$$

where $\mathbf{i}$ is the vector of all ones. Eqs. (13) and (14) together suggest that the force density matrix $\mathbf{E}$ must have a rank deficiency of at least four (i.e., having at least four zero eigenvalues), so as to guarantee that the corresponding tensegrity is three-dimensional, with $\mathbf{x}$, $\mathbf{y}$, $\mathbf{z}$ being linearly independent. Once the connectivity and force densities are provided, the nodal coordinates can be solved from Eq. (13).

In addition to equilibrium, stability is an essential property of pin-jointed frameworks. As described in Appendix A, the specific geometry of a framework, together with certain features of its force densities, may lead to super-stability, namely stability that is independent of the level of prestress in the members. The relevant geometric information is characterized by the geometry matrix $\mathbf{G} \in \mathbb{R}^{b\times 6}$, defined as

$$\mathbf{G} = [\mathbf{U}\mathbf{u}, \mathbf{V}\mathbf{v}, \mathbf{W}\mathbf{w}, \mathbf{U}\mathbf{v}, \mathbf{U}\mathbf{w}, \mathbf{V}\mathbf{w}], \tag{15}$$

which is related to member extensions caused by nontrivial affine motions including stretch and shear (Zhang and Ohsaki, 2015).

3. General theory on duality

3.1. Triangulated polyhedral configurations

Rigid origami consist of rigid polygonal panels connected by hinges. An equivalent pin-jointed framework can be constructed to reproduce the kinematics of the origami. Specifically, the panel edges are replaced by inextensible members connected by ball joints. When all panels are triangles, the resulting framework is kinematically equivalent to the origami, exhibiting the same folding motions. Moreover, if the framework admits a state of self-stress, it constitutes a tensegrity, in which members in tension act as cables and those in compression act as struts. Here, we consider rigid origami in which each crease is shared by two panels and each vertex is incident to several creases. In this setting, the origami corresponds to the 2-skeleton of a polyhedron, a three-dimensional solid bounded by flat polygonal faces, straight edges, and vertices. Correspondingly, the tensegrity corresponds to its 1-skeleton. We note that polyhedra can take rather uncommon forms. For example, they may contain holes, as in toroidal polyhedra, or self-intersecting faces, as in hemipolyhedra. However, the most common polyhedra, such as pyramids and cubes, are homeomorphic to a sphere. That is, they enclose a volume and contain no holes. The duality arises from such polyhedra, as formalized in the following lemma:

Lemma 1. *For a three-dimensional, free-standing tensegrity whose admissible states of self-stress (allowing for possible conversion between struts and cables) span a vector space $\mathbb{S}$ and a three-dimensional, free-standing rigid origami whose admissible infinitesimal mechanisms span a vector space $\mathbb{M}$, if their geometry satisfies*

(a) The tensegrity and the origami are the 1-skeleton and the 2-skeleton of the same polyhedron, respectively;
(b) The polyhedron is homeomorphic to a sphere;
(c) All the faces of the polyhedron are triangles;

then there exists an isomorphism $\mathbf{J} : \mathbb{M} \to \mathbb{S}$, where $\mathbf{J}$ is the Jacobian of the origami dihedral angles with respect to the nodal coordinates.

Proof. According to conditions (a) and (c), the tensegrity and the origami can be described by the same pin-jointed framework. We use $\mathbf{x}, \mathbf{y}, \mathbf{z}$ to denote the nodal coordinates of the framework, $\mathbf{C}$ the connectivity matrix, $\mathbf{D}$ the equilibrium matrix, and $\mathbf{B}$ the kinematic matrix. The null space of $\mathbf{D}$ is $\mathbb{S}$ and the null space of $\mathbf{B}$ is $\mathbb{M} \oplus \overline{\mathbb{R}}$, i.e.,

$$\mathbb{S} = \mathrm{Null}(\mathbf{D}) \quad \text{and} \quad \mathbb{M} \oplus \overline{\mathbb{R}} = \mathrm{Null}(\mathbf{B}), \tag{16}$$

where the space $\overline{\mathbb{R}}$ is spanned by the six independent rigid-body motions. We express $\overline{\mathbb{R}}$ as

$$\overline{\mathbb{R}} = \mathrm{Span}\left\{\mathbf{d}_{\mathrm{t}}^{x}, \mathbf{d}_{\mathrm{t}}^{y}, \mathbf{d}_{\mathrm{t}}^{z}, \mathbf{d}_{\mathrm{r}}^{x}, \mathbf{d}_{\mathrm{r}}^{y}, \mathbf{d}_{\mathrm{r}}^{z}\right\}, \tag{17}$$

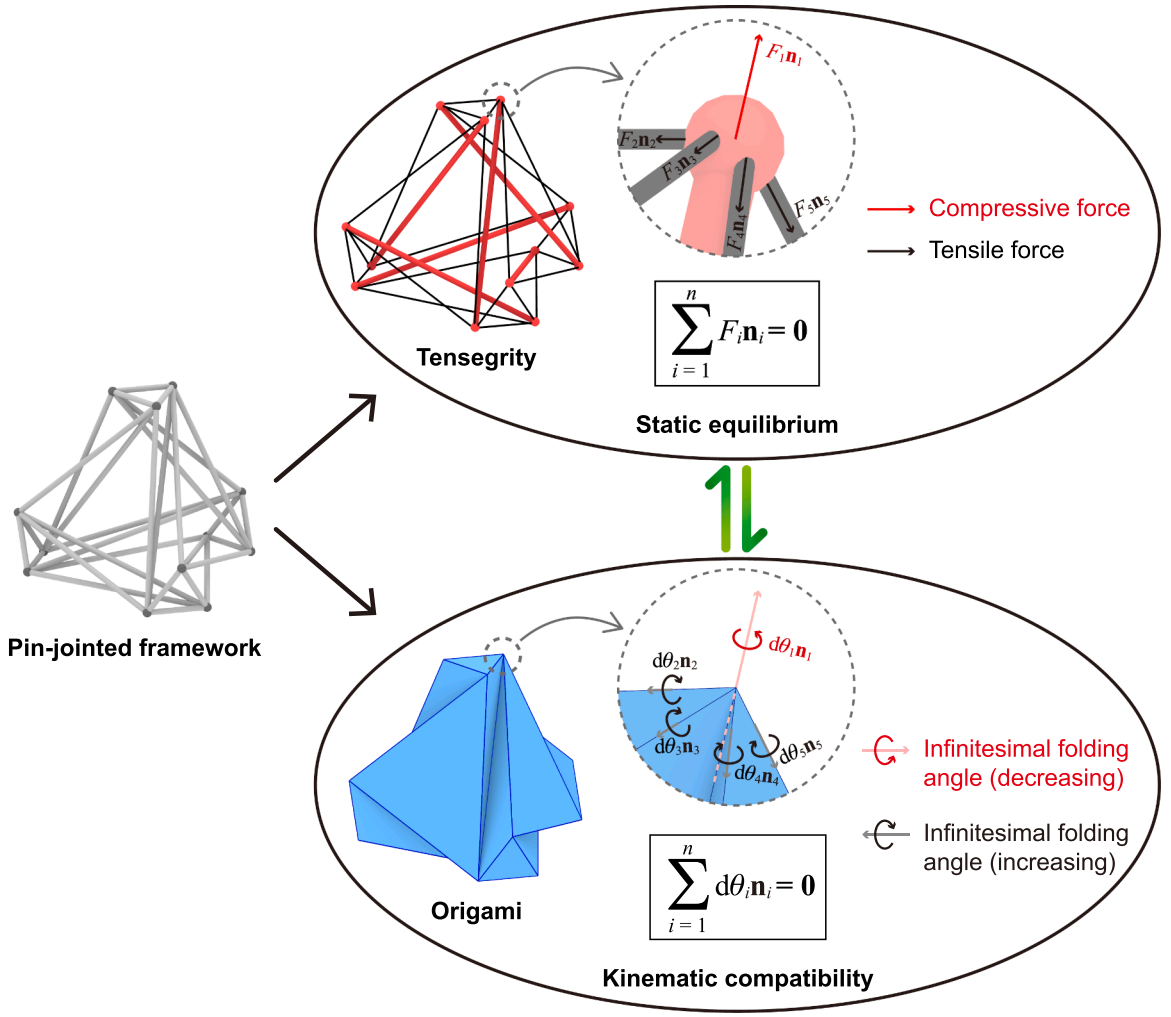

Fig. 1. Duality between the self-stress of tensegrity and the infinitesimal folding mechanisms of origami. The equilibrium statics of the tensegrity and the folding kinematics of the origami can be characterized through the same pin-jointed framework and governed by identical linear equations, expressed in terms of the internal forces F_i and the infinitesimal folding angles (or equivalently the infinitesimal dihedral-angle variations) $\mathrm{d}\theta_i$, respectively. These linear equations are entirely determined by the geometry of the framework, namely the member direction vectors $\mathbf{n}_i$. Positive solutions F_i or $\mathrm{d}\theta_i$ correspond to compressive forces or decreasing dihedral angles, whereas negative solutions correspond to tensile forces or increasing dihedral angles.

where the displacement vectors are given by

$$\mathbf{d}_{\mathrm{t}}^{x}=\begin{bmatrix}\mathbf{i}\\ \mathbf{0}\\ \mathbf{0}\end{bmatrix},\ \mathbf{d}_{\mathrm{t}}^{y}=\begin{bmatrix}\mathbf{0}\\ \mathbf{i}\\ \mathbf{0}\end{bmatrix},\ \mathbf{d}_{\mathrm{t}}^{z}=\begin{bmatrix}\mathbf{0}\\ \mathbf{0}\\ \mathbf{i}\end{bmatrix},\ \mathbf{d}_{\mathrm{r}}^{x}=\begin{bmatrix}\mathbf{0}\\ -\mathbf{z}\\ \mathbf{y}\end{bmatrix},\ \mathbf{d}_{\mathrm{r}}^{y}=\begin{bmatrix}-\mathbf{z}\\ \mathbf{0}\\ \mathbf{x}\end{bmatrix},\ \mathbf{d}_{\mathrm{r}}^{z}=\begin{bmatrix}-\mathbf{y}\\ \mathbf{x}\\ \mathbf{0}\end{bmatrix}, \tag{18}$$

where $\mathbf{i}\in\mathbb{R}^n$ have all the entries equal to 1, and $\mathbf{0}\in\mathbb{R}^n$ have all the entries equal to 0. The first three vectors $\mathbf{d}_{\mathrm{t}}^{x}$, $\mathbf{d}_{\mathrm{t}}^{y}$, and $\mathbf{d}_{\mathrm{t}}^{z}$ represent the translations in the x, y, and z direction, respectively. The last three vectors $\mathbf{d}_{\mathrm{r}}^{x}$, $\mathbf{d}_{\mathrm{r}}^{y}$, and $\mathbf{d}_{\mathrm{r}}^{z}$ represent the infinitesimal rotations around the x, y, and z axis, respectively. The framework is three-dimensional, which means $\mathbf{x}$, $\mathbf{y}$, $\mathbf{z}$, and $\mathbf{i}$ are linearly independent. Thus, the space $\overline{\mathbb{R}}$ has dimension 6. We let d_m denote the dimension of $\mathbb{M}$. Considering $\mathbb{M}\cap\overline{\mathbb{R}}=\{\mathbf{0}\}$, the dimension of $\mathbb{M}\oplus\overline{\mathbb{R}}$ is d_m+6. We let d_s denote the dimension of $\mathbb{S}$. From the viewpoint of structural mechanics, d_s is the number of independent states of self-stress for the tensegrity, and d_m is the number of independent infinitesimal mechanisms for the origami. The generalized Maxwell counting rule gives (Maxwell, 1864; Pellegrino and Calladine, 1986)

$$d_s-(d_m+6)=b-3n. \tag{19}$$

Conditions (b) and (c) lead to the following two combinatorial relationships. First, since the polyhedron is homeomorphic to a sphere, the Euler characteristic χ equals 2, i.e.,

$$\chi=n-b+f=2. \tag{20}$$

Table 1
Correspondence between internal forces of tensegrity and infinitesimal dihedral-angle variations of origami.

Tensegrity	Origami
Compressive force	Decreasing dihedral angle
Tensile force	Increasing dihedral angle
Zero force	Fixed dihedral angle

Second, since the polyhedron is triangulated, the edge number b and the face number f satisfy

$$3f = 2b. \tag{21}$$

Combining Eqs. (19)–(21), we obtain

$$d_s = d_m. \tag{22}$$

Eq. (22) means that the vector spaces $\mathbb{S}$ and $\mathbb{M}$ have the same dimension. Next, we build the isomorphism from $\mathbb{M}$ to $\mathbb{S}$. We use $\mathbf{m}_k$ $(k = 1, 2, \ldots, d_m)$ to denote d_m linearly independent infinitesimal mechanisms of the origami, such that

$$\mathbb{M} = \text{Span}\left\{\mathbf{m}_1, \mathbf{m}_2, \ldots, \mathbf{m}_{d_m}\right\}. \tag{23}$$

The infinitesimal mechanisms $\mathbf{m}_k$ do not involve the first-order elongation of any member of the framework. As a result, the deformation caused by $\mathbf{m}_k$ is purely the first-order rotations between triangular faces, corresponding to the dihedral-angle variations, also known as folding angles. If there is neither the elongation nor the rotation, the mechanisms $\mathbf{m}_k$ degenerate to rigid-body motions in $\overline{\mathbb{R}}$. We denote by $\boldsymbol{\theta}$ the array of dihedral angles, and $\mathbf{J} \in \mathbb{R}^{b\times 3n}$ the Jacobian of $\boldsymbol{\theta}$ with respect to $\mathbf{x}$, $\mathbf{y}$, and $\mathbf{z}$. Then, we have

$$\mathbf{J} = \left[\frac{\partial \boldsymbol{\theta}}{\partial \mathbf{x}}, \frac{\partial \boldsymbol{\theta}}{\partial \mathbf{y}}, \frac{\partial \boldsymbol{\theta}}{\partial \mathbf{z}}\right] \quad \text{and} \quad (\mathrm{d}\boldsymbol{\theta})_k = \mathbf{J}\mathbf{m}_k, \tag{24}$$

for $k = 1, 2, \ldots, d_m$, where the vector $(\mathrm{d}\boldsymbol{\theta})_k$ contains the infinitesimal dihedral-angle variation related to the infinitesimal mechanism $\mathbf{m}_k$. The Jacobian $\mathbf{J}$ has been well defined and formulated by Liu and Paulino (2017) (see Fig. 4 and Equations (2.33)– (2.36) therein; also given by Eq. (D.16)). As discussed in the work of Tachi (2012), the infinitesimal mechanisms $\mathbf{m}_k$ preserve the closed loop of faces around each node, which can be expressed by

$$\mathbf{D}(\mathrm{d}\boldsymbol{\theta})_k = \mathbf{D}\mathbf{J}\mathbf{m}_k = \mathbf{0}. \tag{25}$$

In terms of origami folding kinematics, Eq. (25) means that the *angular velocities* along creases sum up to zero at each node. In other words, the infinitesimal mechanism $\mathbf{m}_k$ does not tear up the origami. It is important to point out that the vectors $\mathbf{J}\mathbf{m}_k$ $(k = 1, 2, \ldots, d_m)$ are linearly independent. This can be proved by assuming that they are linearly dependent. Then, there exist scalars c_k $(k = 1, 2, \ldots, d_m)$, not all zero, such that $\sum_{k=1}^{d_m}(c_k\mathbf{J}\mathbf{m}_k) = \mathbf{J}\sum_{k=1}^{d_m}(c_k\mathbf{m}_k) = \mathbf{0}$. However, since $\mathbf{m}_k$ $(k = 1, 2, \ldots, d_m)$ are linearly independent, $\sum_{k=1}^{d_m}(c_k\mathbf{m}_k)$ is a nonzero infinitesimal mechanism (not rigid-body motions), and therefore, it must induce nonzero first-order variation of $\boldsymbol{\theta}$, which is contradictory to $\mathbf{J}\sum_{k=1}^{d_m}(c_k\mathbf{m}_k) = \mathbf{0}$. Considering the dimension equality $d_s = d_m$, the linearly independent vectors $\mathbf{J}\mathbf{m}_k$ $(k = 1, 2, \ldots, d_s)$ form a basis of $\mathbb{S}$, such that

$$\mathbb{S} = \text{Span}\left\{\mu\mathbf{J}\mathbf{m}_1, \mu\mathbf{J}\mathbf{m}_2, \ldots, \mu\mathbf{J}\mathbf{m}_{d_s}\right\}. \tag{26}$$

Here, the coefficient μ is a nonzero scalar with units of N, ensuring dimensional consistency: vectors in $\mathbb{S}$ must have units of N while $\mathbf{J}\mathbf{m}_i$ is dimensionless. Meanwhile, in terms of tensegrity, for any state of self-stress $\mathbf{s} \in \mathbb{S}$, there exist unique scalars c_k $(k = 1, 2, \ldots, d_s)$, such that

$$\mathbf{s} = \sum_{k=1}^{d_s}(c_k\mu\mathbf{J}\mathbf{m}_k) = \mathbf{J}\sum_{k=1}^{d_s}(c_k\mu\mathbf{m}_k). \tag{27}$$

The uniqueness is owing to the fact that $\mathbf{J}\mathbf{m}_k$ $(k = 1, 2, \ldots, d_s)$ are linearly independent. In addition, $\sum_{k=1}^{d_s}(c_k\mathbf{m}_k)$ is a unique vector in $\mathbb{M}$, since $\mathbf{m}_k$ $(k = 1, 2, \ldots, d_s)$ are linearly independent. As a result, $\mathbf{J}$ is an *onto* and *one-to-one* linear transformation from $\mathbb{M}$ to $\mathbb{S}$. That is to say, $\mathbf{J} : \mathbb{M} \to \mathbb{S}$ is an isomorphism. □

Under the three conditions stated in Lemma 1, the space of states of self-stress of the tensegrity and the space of infinitesimal mechanisms of the origami are isomorphic. We refer to this isomorphic correspondence as the *duality of tensegrity and origami*. Fig. 1 illustrates this duality through the example of a truncated tetrahedral tensegrity and its dual origami. According to the duality relationship, a compressive tensegrity member i, i.e., a strut, corresponds to an origami crease i with a decreasing dihedral angle, since both F_i and $\mathrm{d}\theta_i$ are negative. Likewise, a tensile tensegrity member, i.e., a cable, corresponds to an increasing dihedral angle, with F_i and $\mathrm{d}\theta_i$ being positive. These correspondences are summarized in Table 1. As a special case, a zero internal force is associated with a fixed dihedral angle, consistent with the constrained auxiliary members introduced later for general polyhedral configurations. Empirically, one may place struts along valley creases and cables along mountain creases. This strut-cable assignment is likely to be consistent with the signs of the dihedral-angle variations, as observed in all examples presented in this paper. However, such consistency is not guaranteed in general, as remarked by Tachi (2012). We also note that the signs of the internal forces or folding

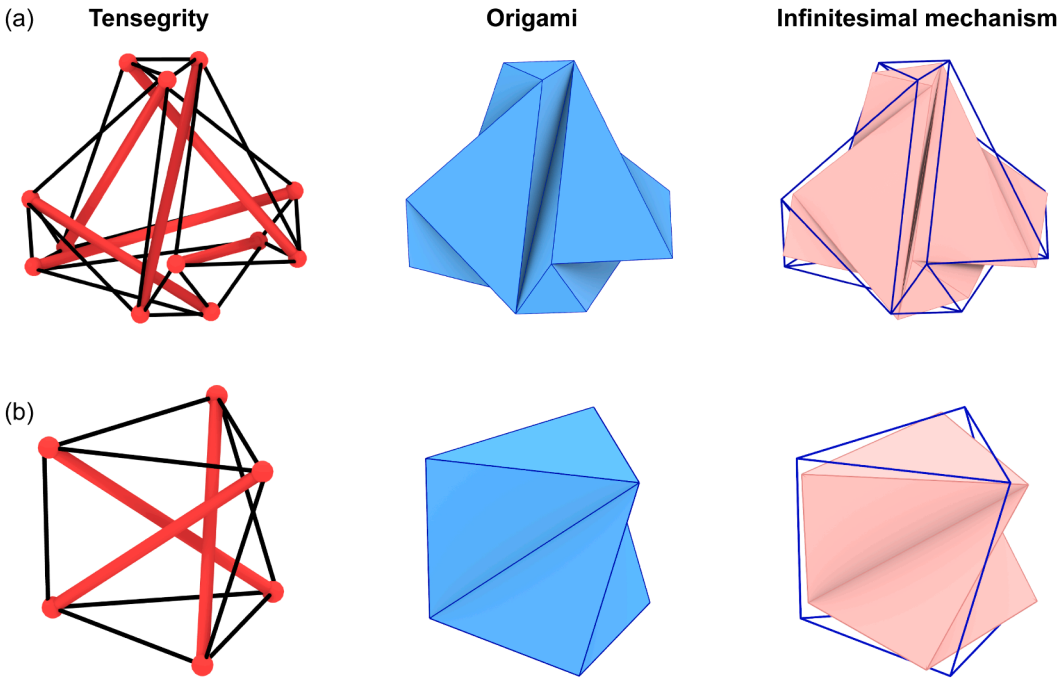

Fig. 2. Dual configurations of tensegrity (left column) and origami (middle column), together with the corresponding infinitesimal mechanisms (right column). The blue lines indicate the undeformed outlines. (a) Rhombic tetrahedral configuration. (b) Triangular prismatic configuration.

angles are subject to a global reversal under the duality relationship. For example, reversing all the folding angles associated with a shrinking deformation of a polyhedral origami results in an expanding deformation of the same mechanism. In this case, all the decreasing dihedral angles are paired with tensile forces in the dual tensegrity and all the increasing dihedral angles are paired with compressive forces. Similarly, reversing all the internal forces in a tensegrity, i.e., exchanging struts and cables, preserves self-equilibrium. However, this reversal may affect the stability of the tensegrity. Therefore, when constructing a tensegrity from origami, one must further examine the stability of the resulting tensegrity under the prescribed strut-cable assignment. By contrast, constructing a flexible origami from a tensegrity is more straightforward, as stability is not an issue for the origami counterpart.

The truncated tetrahedral tensegrity belongs to a broader family of super-stable tensegrities, known as *rhombic truncated regular polyhedral (TRP) tensegrities*, originally discovered by Zhang et al. (2013). Although the underlying polyhedral geometry admits infinitesimal mechanisms, these tensegrities remain stable due to the existence of self-stress. Specifically, infinitesimal deformations are resisted because they induce negative work by the internal forces and an increase in the total potential energy from a local minimum, a phenomenon referred to as *prestress stability*. Prestress-stable tensegrities, however, may lose stability when the axial stiffness of the members is small and the level of force densities is high. By contrast, certain tensegrities, including the rhombic TRP tensegrities, are super-stable, meaning that stability is guaranteed regardless of material properties or prestress levels. A set of sufficient conditions for super-stability is provided in Appendix A, in terms of the geometric matrix $\mathbf{G}$ and the force density matrix $\mathbf{E}$. The condition involving $\mathbf{G}$ is equivalent to a geometric constraint requiring that the member direction vectors of the tensegrity do not lie on a common conic at infinity, a condition that is rarely violated in practice. In addition, if the force density matrix $\mathbf{E}$ is positive semi-definite and has a rank deficiency of four, the tensegrity is super-stable. For rhombic TRP tensegrities, the force densities are given explicitly by Zhang et al. (2013) (see also Appendix B and Fig. A.8), and can be proved to satisfy the super-stability conditions.

The infinitesimally flexible origami that is dual to the truncated tetrahedral tensegrity turns out to be a variant with different edge lengths from Jessen's icosahedron (Jessen, 1967), the dual counterpart of the six-bar icosahedral tensegrity invented by Kenneth Snelson in 1949 (Cera, 2020). The infinitesimal mechanism vector $\mathbf{m}$ of the truncated tetrahedral origami can be obtained by solving Eq. (8) and is shown in Fig. 2(a), right. The duality theory can be validated by computing $\mathbf{Jm}$ and checking $\mathbf{DJm} = \mathbf{0}$. Fig. 2(b) shows another dual pair of tensegrity and origami that have triangulated configurations. The tensegrity shown is the simplest one-layer tower with triangular bases, invented by Karl Ioganson in 1921 (Bansod et al., 2014). It belongs to the broader class of multilayer tensegrity towers (Snelson, 1965; Sultan, 1999; Nishimura, 2000; Tibert, 2002). Based on the mathematical development of Nishimura (2000), we derive explicit expressions for the force densities of these multilayer tensegrity towers and demonstrate that they are super-stable over a broad range of overlap ratios between adjacent layers. The detailed analysis is provided in Appendix C, and Figs. C.9–C.16. Once again, Lemma 1 determines the corresponding infinitesimally flexible dual origami, namely Schönhardt's octahedron (Schönhardt, 1928).

3.2. General polyhedral configurations

The triangulation condition (c) in Lemma 1 is fundamental to establishing the isomorphism with the dimension equivalence $d_s = d_m$. However, many tensegrity and origami configurations that potentially exhibit this dual relationship are not triangulated. For instance, the one-layer prismatic tensegrity and origami (Fig. 4, $n = 1$) share the same chiral geometry, which has been extensively studied in the context of Kresling origami (Kresling, 2008; Lu et al., 2022; Zang et al., 2024). Although much attention has focused on the bistability of Kresling origami (Zang et al., 2024), certain geometric configurations admit only a single infinitesimally flexible state (Appendix D), which corresponds precisely to the unique state of self-stress of the associated prismatic tensegrity (Appendix C.1.1). We refer to Dang and Paulino (2026) (Fig. 5 therein) for a comparison between infinitesimally flexible and multistable Kresling origami, which exhibit distinct energy landscapes under compression.

To investigate the duality of tensegrity and origami for general polyhedral geometries, we append diagonals to the polygonal faces to obtain a triangulation of the underlying polyhedron, thereby enabling the application of Lemma 1. The appended diagonals become *auxiliary members* in the associated pin-jointed framework. The definition of auxiliary members is given as follows:

Definition 1. An auxiliary member is an additional member appended to a pin-jointed framework that may sustain internal force under the tensegrity interpretation or act as a foldable edge under the origami interpretation.

Lemma 1 applies to pin-jointed frameworks triangulated by auxiliary members. The triangular faces are resistant to bending, making such frameworks well suited for modeling rigid origami (Chen and Santangelo, 2018; McInerney et al., 2020). However, the addition of members may generate extra states of self-stress or eliminate infinitesimal mechanisms, as indicated by Eq. (19) through the increase in b. The impact of such triangulation on the resulting duality relationship therefore warrants further analysis. To this end, we introduce the notion of *constrained auxiliary members (CAMs)*:

Definition 2. A constrained auxiliary member (CAM) is an auxiliary member that carries zero internal force under the tensegrity interpretation or has zero first-order dihedral-angle variation under the origami interpretation.

In this manner, the origami exhibits the same kinematics as its pin-jointed framework augmented with CAMs. Meanwhile, the CAMs does not alter the state of self-stress of the tensegrity, since these members carry zero internal force. Accordingly, the duality of tensegrity and origami for general polyhedral geometries can be investigated in two steps. First, auxiliary members are appended to achieve triangulation, thereby enabling Lemma 1 to apply to the expanded spaces of states of self-stress and infinitesimal mechanisms. Second, the auxiliary members are converted into CAMs, allowing the actual spaces of states of self-stress and infinitesimal mechanisms to be identified. Based on the above considerations, we propose and prove the following theorem:

Theorem 1. *For a three-dimensional, free-standing tensegrity whose admissible states of self-stress (allowing for possible conversion between struts and cables) span a vector space $\mathbb{S}$ and a three-dimensional, free-standing rigid origami whose admissible infinitesimal mechanisms span a vector space $\mathbb{M}$, if their geometry satisfies*

(a) The tensegrity and the origami are the 1-skeleton and the 2-skeleton of the same polyhedron, respectively;
(b) The polyhedron is homeomorphic to a sphere;

then there exists an isomorphism $\mathbf{J} : \mathbb{M} \to \mathbb{S}$, where $\mathbf{J}$ is the Jacobian of the origami dihedral angles with respect to the nodal coordinates.

Proof. If the polyhedron consists solely of triangular faces, the theorem reduces directly to Lemma 1 and therefore holds. For a polyhedron with general polygonal faces, we triangulate each face by inserting diagonals. Correspondingly, auxiliary members are added along these diagonals, yielding a triangulated framework. Let the original framework have b members and n nodes, and suppose $\bar{b}$ auxiliary members are introduced. The total number of members is $\hat{b} = b + \bar{b}$. For the original framework, denote by $\mathbf{C} \in \mathbb{R}^{b\times n}$, $\mathbf{B} \in \mathbb{R}^{b\times 3n}$, and $\mathbf{D} \in \mathbb{R}^{3n\times b}$ the connectivity, kinematic, and equilibrium matrices, respectively. The associated diagonal matrices of coordinate differences and lengths are $\mathbf{U}$, $\mathbf{V}$, $\mathbf{W}$, $\mathbf{L} \in \mathbb{R}^{b\times b}$. Since the tensegrity corresponds to the 1-skeleton of the original (non-triangulated) polyhedron, its space of self-stress is

$$\boxed{\mathbb{S} = \mathrm{Null}(\mathbf{D}).} \tag{28}$$

In contrast, the origami interpretation of the 2-skeleton imposes additional kinematic constraints. These arise from the auxiliary members and lead to

$$\mathbb{M} \oplus \overline{\mathbb{R}} \subseteq \mathrm{Null}(\mathbf{B}), \tag{29}$$

where $\overline{\mathbb{R}}$ denotes rigid-body motions. The auxiliary members do not modify the nodal coordinates $\mathbf{x}, \mathbf{y}, \mathbf{z}$ of the original framework; rather, they contribute additional rows to the connectivity matrix, denoted by $\overline{\mathbf{C}} \in \mathbb{R}^{\bar{b}\times n}$. The $\bar{k}$-th row of $\overline{\mathbf{C}}$ corresponds to the auxiliary member connecting nodes i and j, whose p-th entry is defined as

$$\overline{C}_{\bar{k},p} = \begin{cases} \mathrm{sign}(j-p), & \text{if } \ p = i; \\ \mathrm{sign}(i-p), & \text{if } \ p = j; \\ 0, & \text{otherwise}, \end{cases} \tag{30}$$

for $\bar{k} = 1, 2, \ldots, \bar{b}$ and $p = 1, 2, \ldots, n$. The additional coordinate difference vectors $\overline{\mathbf{u}}$, $\overline{\mathbf{v}}$, $\overline{\mathbf{w}} \in \mathbb{R}^{\bar{b}}$ are given by

$$\overline{\mathbf{u}} = \overline{\mathbf{C}}\mathbf{x}, \quad \overline{\mathbf{v}} = \overline{\mathbf{C}}\mathbf{y}, \quad \overline{\mathbf{w}} = \overline{\mathbf{C}}\mathbf{z}. \tag{31}$$

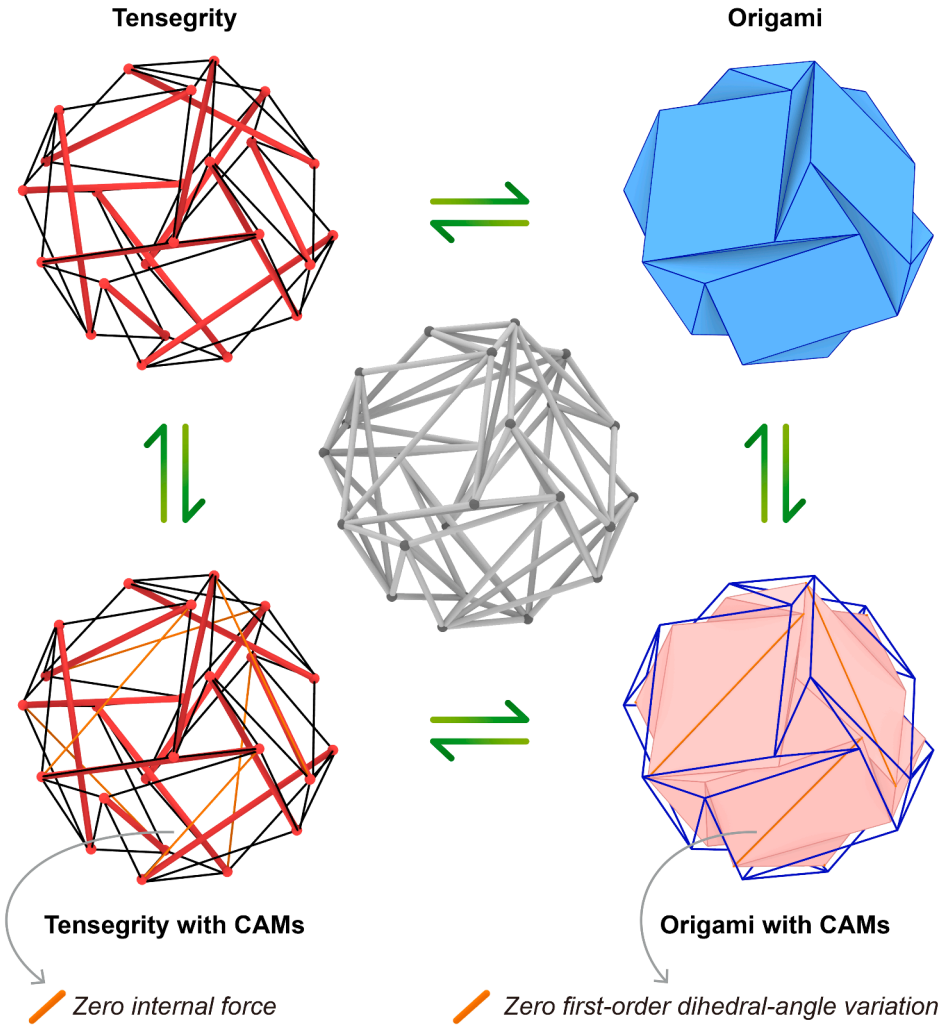

Fig. 3. The triangulation construction revealing duality between the self-stress and the infinitesimal folding mechanisms. The blue lines indicate the undeformed outlines. The equilibrium statics of the tensegrity and the folding kinematics of the origami can be characterized within the same triangulated pin-jointed framework, obtained by introducing diagonals into non-triangular faces. These additional diagonals, referred to as constrained auxiliary members, carry zero internal force in the tensegrity and undergo zero extension and zero dihedral-angle variation in the origami. This construction yields an equivalent geometric interpretation of the pin-jointed framework for both self-stressed tensegrities and shaky origami.

The auxiliary member lengths $\bar{\mathbf{l}} \in \mathbb{R}^{\bar{b}}$ have components

$$\bar{\ell}_{\bar{k}} = \sqrt{\bar{u}_{\bar{k}}^2 + \bar{v}_{\bar{k}}^2 + \bar{w}_{\bar{k}}^2}, \tag{32}$$

for $\bar{k} = 1, 2, \ldots, \bar{b}$, where $\bar{u}_{\bar{k}}$, $\bar{v}_{\bar{k}}$, $\bar{w}_{\bar{k}}$ are the $\bar{k}$-th components of $\overline{\mathbf{u}}$, $\overline{\mathbf{v}}$, $\overline{\mathbf{w}}$, respectively. The corresponding diagonal matrices are defined as

$$\overline{\mathbf{U}} = \operatorname{diag}(\overline{\mathbf{u}}), \quad \overline{\mathbf{V}} = \operatorname{diag}(\overline{\mathbf{v}}), \quad \overline{\mathbf{W}} = \operatorname{diag}(\overline{\mathbf{w}}), \quad \overline{\mathbf{L}} = \operatorname{diag}(\bar{\mathbf{l}}), \tag{33}$$

all in $\mathbb{R}^{\bar{b}\times\bar{b}}$. The additional kinematic matrix $\overline{\mathbf{B}} \in \mathbb{R}^{\bar{b}\times 3n}$ and the additional equilibrium matrix $\overline{\mathbf{D}} \in \mathbb{R}^{3n\times\bar{b}}$ are then expressed as

$$\overline{\mathbf{B}} = \begin{bmatrix} \overline{\mathbf{L}}^{-1}\overline{\mathbf{U}}\overline{\mathbf{C}} & \overline{\mathbf{L}}^{-1}\overline{\mathbf{V}}\overline{\mathbf{C}} & \overline{\mathbf{L}}^{-1}\overline{\mathbf{W}}\overline{\mathbf{C}} \end{bmatrix} \text{ and } \overline{\mathbf{D}} = \overline{\mathbf{B}}^{\mathrm{T}} = \begin{bmatrix} \overline{\mathbf{C}}^{\mathrm{T}}\overline{\mathbf{U}}\overline{\mathbf{L}}^{-1} \\ \overline{\mathbf{C}}^{\mathrm{T}}\overline{\mathbf{V}}\overline{\mathbf{L}}^{-1} \\ \overline{\mathbf{C}}^{\mathrm{T}}\overline{\mathbf{W}}\overline{\mathbf{L}}^{-1} \end{bmatrix}, \tag{34}$$

respectively. After incorporating the auxiliary members, the overall connectivity matrix $\widehat{\mathbf{C}} \in \mathbb{R}^{(b+\bar{b})\times n}$, kinematic matrix $\widehat{\mathbf{B}} \in \mathbb{R}^{(b+\bar{b})\times 3n}$, and equilibrium matrix $\widehat{\mathbf{D}} \in \mathbb{R}^{3n\times(b+\bar{b})}$ become

$$\widehat{\mathbf{C}} = \begin{bmatrix} \mathbf{C} \\ \overline{\mathbf{C}} \end{bmatrix}, \quad \widehat{\mathbf{B}} = \begin{bmatrix} \mathbf{B} \\ \overline{\mathbf{B}} \end{bmatrix}, \quad \text{and} \quad \widehat{\mathbf{D}} = \begin{bmatrix} \mathbf{D} & \overline{\mathbf{D}} \end{bmatrix}, \tag{35}$$

respectively. Let

$$\widehat{\mathbb{S}} = \text{Null}(\widehat{\mathbf{D}}) \quad \text{and} \quad \widehat{\mathbb{M}} \oplus \overline{\mathbb{R}} = \text{Null}(\widehat{\mathbf{B}}). \tag{36}$$

By Lemma 1, there exists an isomorphism

$$\widehat{\mathbf{J}} : \widehat{\mathbb{M}} \to \widehat{\mathbb{S}}, \tag{37}$$

where $\widehat{\mathbf{J}} \in \mathbb{R}^{(b+\bar{b})\times 3n}$ is the Jacobian of the dihedral angles with respect to the nodal coordinates. Let the vector $\boldsymbol{\theta}$ collect the dihedral angles associated with the original members and $\bar{\boldsymbol{\theta}}$ those associated with the auxiliary members. We denote their Jacobians by $\mathbf{J} \in \mathbb{R}^{b\times 3n}$ and $\overline{\mathbf{J}} \in \mathbb{R}^{\bar{b}\times 3n}$. Then it follows that

$$\widehat{\mathbf{J}} = \begin{bmatrix} \mathbf{J} \\ \overline{\mathbf{J}} \end{bmatrix}, \quad \mathbf{J} = \begin{bmatrix} \dfrac{\partial \boldsymbol{\theta}}{\partial \mathbf{x}}, \dfrac{\partial \boldsymbol{\theta}}{\partial \mathbf{y}}, \dfrac{\partial \boldsymbol{\theta}}{\partial \mathbf{z}} \end{bmatrix}, \quad \text{and} \quad \overline{\mathbf{J}} = \begin{bmatrix} \dfrac{\partial \bar{\boldsymbol{\theta}}}{\partial \mathbf{x}}, \dfrac{\partial \bar{\boldsymbol{\theta}}}{\partial \mathbf{y}}, \dfrac{\partial \bar{\boldsymbol{\theta}}}{\partial \mathbf{z}} \end{bmatrix}, \quad \text{with } \mathrm{d}\boldsymbol{\theta} = \mathbf{J}\hat{\mathbf{m}} \text{ and } \mathrm{d}\bar{\boldsymbol{\theta}} = \overline{\mathbf{J}}\hat{\mathbf{m}}, \tag{38}$$

for $\hat{\mathbf{m}} \in \widehat{\mathbb{M}}$. Under the origami interpretation, the CAM constraint is

$$\mathrm{d}\bar{\boldsymbol{\theta}} = \overline{\mathbf{J}}\hat{\mathbf{m}} = \bar{\mathbf{0}}. \tag{39}$$

Here, we specifically use $\bar{\mathbf{0}}$ to denote the zero vector of the same size as $\mathrm{d}\bar{\boldsymbol{\theta}}$. Defining the expanded kinematic matrix $\widetilde{\mathbf{B}} \in \mathbb{R}^{(b+2\bar{b})\times 3n}$ as

$$\widetilde{\mathbf{B}} = \begin{bmatrix} \widehat{\mathbf{B}} \\ \overline{\mathbf{J}} \end{bmatrix}, \tag{40}$$

the space of infinitesimal folding mechanisms $\mathbb{M}$ is characterized by

$$\boxed{\mathbb{M} \oplus \overline{\mathbb{R}} = \text{Null}\left(\widetilde{\mathbf{B}}\right).} \tag{41}$$

In this way, the dihedral angles associated with the auxiliary members are fixed to zero, prohibiting bending of origami panels. We suppose that the origami has d_m independent infinitesimal mechanisms $\mathbf{m}_k$ $(k = 1, 2, \ldots, d_m)$. They satisfy $\widetilde{\mathbf{B}}\mathbf{m}_k = \mathbf{0}$ and span the space $\mathbb{M}$:

$$\mathbb{M} = \text{Span}\left\{ \mathbf{m}_1, \ldots, \mathbf{m}_{d_m} \right\}. \tag{42}$$

Let $\hat{d}_m = \dim \widehat{\mathbb{M}}$. Then there exists an $(\hat{d}_m - d_m)$-dimensional complementary subspace $\overline{\mathbb{M}}$, such that

$$\widehat{\mathbb{M}} = \mathbb{M} \oplus \overline{\mathbb{M}} \quad \text{and} \quad \mathbb{M} \cap \overline{\mathbb{M}} = \mathbf{0}. \tag{43}$$

We denote by $\overline{\mathbf{m}}_{\bar{k}}$ $(\bar{k} = 1, 2, \ldots, \hat{d}_m - d_m)$ a basis of $\overline{\mathbb{M}}$:

$$\overline{\mathbb{M}} = \text{Span}\left\{ \overline{\mathbf{m}}_1, \overline{\mathbf{m}}_2, \ldots, \overline{\mathbf{m}}_{\hat{d}_m - d_m} \right\}. \tag{44}$$

The infinitesimal mechanisms $\mathbf{m}_k$ $(k = 1, 2, \ldots, d_m)$ and $\overline{\mathbf{m}}_{\bar{k}}$ $(\bar{k} = 1, 2, \ldots, \hat{d}_m - d_m)$ form a basis of the $\hat{d}_m$-dimensional space $\widehat{\mathbb{M}}$:

$$\widehat{\mathbb{M}} = \text{Span}\left\{ \mathbf{m}_1, \mathbf{m}_2, \ldots, \mathbf{m}_{d_m}, \overline{\mathbf{m}}_1, \overline{\mathbf{m}}_2, \ldots, \overline{\mathbf{m}}_{\hat{d}_m - d_m} \right\}. \tag{45}$$

The vectors $\overline{\mathbf{m}}_{\bar{k}}$ preserve all member lengths of the triangulated framework but induce bending of polygonal faces in the origami, whereas $\mathbf{m}_k$ induce neither stretching nor bending. Since $\mathbb{M} \cap \overline{\mathbb{M}} = \mathbf{0}$, we have

$$\sum_{\bar{k}=1}^{\hat{d}_m - d_m} \left(\bar{c}_{\bar{k}} \overline{\mathbf{J}}\overline{\mathbf{m}}_{\bar{k}} \right) \neq \bar{\mathbf{0}}, \tag{46}$$

for any coefficients $\bar{c}_{\bar{k}}$ $(\bar{k} = 1, 2, \ldots, \hat{d}_m - d_m)$ not all zero. Let $\hat{d}_s = \dim \widehat{\mathbb{S}}$. The isomorphism $\widehat{\mathbf{J}} : \widehat{\mathbb{M}} \to \widehat{\mathbb{S}}$ implies

$$\hat{d}_s = \hat{d}_m, \tag{47}$$

and the vectors $\widehat{\mathbf{J}}\mathbf{m}_k$ $(k = 1, 2, \ldots, d_m)$ and $\widehat{\mathbf{J}}\overline{\mathbf{m}}_{\bar{k}}$ $(\bar{k} = 1, 2, \ldots, \hat{d}_s - d_m)$ span $\widehat{\mathbb{S}}$:

$$\widehat{\mathbb{S}} = \text{Span}\left\{ \mu\widehat{\mathbf{J}}\mathbf{m}_1, \mu\widehat{\mathbf{J}}\mathbf{m}_2, \ldots, \mu\widehat{\mathbf{J}}\mathbf{m}_{d_m}, \mu\widehat{\mathbf{J}}\overline{\mathbf{m}}_1, \mu\widehat{\mathbf{J}}\overline{\mathbf{m}}_2, \ldots, \mu\widehat{\mathbf{J}}\overline{\mathbf{m}}_{\hat{d}_s - d_m} \right\}. \tag{48}$$

For any state of self-stress $\mathbf{s} \in \mathbb{S}$, we have

$$\widehat{\mathbf{D}} \begin{bmatrix} \mathbf{s} \\ \bar{\mathbf{0}} \end{bmatrix} = \mathbf{D}\mathbf{s} + \overline{\mathbf{D}}\bar{\mathbf{0}} = \mathbf{0}. \tag{49}$$

That is to say,

$$\begin{bmatrix}\mathbf{s}\\ \bar{\mathbf{0}}\end{bmatrix} \in \hat{\mathbb{S}}, \tag{50}$$

and therefore it admits a unique decomposition in terms of the above basis. Specifically, there exist unique scalars c_k ($k = 1, 2, \ldots, \hat{d}_s$), such that

$$\begin{aligned}\begin{bmatrix}\mathbf{s}\\ \bar{\mathbf{0}}\end{bmatrix} &= \sum_{k=1}^{d_m}\left(c_k\mu\hat{\mathbf{J}}\mathbf{m}_k\right) + \sum_{\bar{k}=1}^{\hat{d}_s-d_m}\left(c_{\bar{k}+d_m}\mu\hat{\mathbf{J}}\overline{\mathbf{m}}_{\bar{k}}\right)\\ &= \sum_{k=1}^{d_m}\left(c_k\begin{bmatrix}\mu\mathbf{J}\mathbf{m}_k\\ \mu\bar{\mathbf{J}}\mathbf{m}_k\end{bmatrix}\right) + \sum_{\bar{k}=1}^{\hat{d}_s-d_m}\left(c_{\bar{k}+d_m}\begin{bmatrix}\mu\mathbf{J}\overline{\mathbf{m}}_{\bar{k}}\\ \mu\bar{\mathbf{J}}\overline{\mathbf{m}}_{\bar{k}}\end{bmatrix}\right)\\ &= \sum_{k=1}^{d_m}\left(c_k\begin{bmatrix}\mu\mathbf{J}\mathbf{m}_k\\ \bar{\mathbf{0}}\end{bmatrix}\right) + \sum_{\bar{k}=1}^{\hat{d}_s-d_m}\left(c_{\bar{k}+d_m}\begin{bmatrix}\mu\mathbf{J}\overline{\mathbf{m}}_{\bar{k}}\\ \mu\bar{\mathbf{J}}\overline{\mathbf{m}}_{\bar{k}}\end{bmatrix}\right).\end{aligned} \tag{51}$$

Eqs. (46) and (51) yield $c_{\bar{k}+d_m} = 0$ ($\bar{k} = 1, 2, \ldots, \hat{d}_m - d_m$). Therefore, there exist unique scalars c_k ($k = 1, 2, \ldots, d_m$), such that

$$\mathbf{s} = \sum_{k=1}^{d_m}(c_k\mu\mathbf{J}\mathbf{m}_k) = \mu\mathbf{J}\sum_{k=1}^{d_m}(c_k\mathbf{m}_k), \tag{52}$$

where $\sum_{k=1}^{d_m}(c_k\mathbf{m}_k)$ is a unique vector in $\mathbb{M}$. Moreover, for any $\mathbf{m} \in \mathbb{M}$,

$$\hat{\mathbf{J}}\mathbf{m} = \begin{bmatrix}\mathbf{J}\mathbf{m}\\ \bar{\mathbf{J}}\mathbf{m}\end{bmatrix} = \begin{bmatrix}\mathbf{J}\mathbf{m}\\ \bar{\mathbf{0}}\end{bmatrix}, \tag{53}$$

so that $\mathbf{J}\mathbf{m} \in \mathbb{S}$. This establishes a one-to-one correspondence between vectors in $\mathbb{S}$ and $\mathbb{M}$. Let $d_s = \dim\mathbb{S}$. We have

$$d_s = d_m, \tag{54}$$

and the linearly independent vectors $\mathbf{J}\mathbf{m}_k$ ($k = 1, 2, \ldots, d_s$) span $\mathbb{S}$:

$$\mathbb{S} = \mathrm{Span}\left\{\mu\mathbf{J}\mathbf{m}_1, \mu\mathbf{J}\mathbf{m}_2, \ldots, \mu\mathbf{J}\mathbf{m}_{d_s}\right\}. \tag{55}$$

Altogether, $\mathbf{J} : \mathbb{M} \to \mathbb{S}$ is an isomorphism. □

Theorem 1 demonstrates that the duality between tensegrity and origami fundamentally arises from their shared polyhedral geometry. The homeomorphism to a sphere implies an Euler characteristic $\chi = 2$, which leads to equal dimensions of the stress and mechanism spaces, $d_s = d_m$. This becomes clearer by rewriting the counting rule as $d_s - d_m = 6 - 3\chi = 0$ for triangulated polyhedra. If the framework is not homeomorphic to a sphere, the duality may not hold. For example, a triangulation of a torus, also referred to as a toroidal polyhedron, has $\chi = 0$. In this case, the counting rule becomes $d_s - d_m = 6 - 3\chi = 6$, indicating a mismatch between the dimensions of the stress and mechanism spaces and hence the loss of duality. This mismatch is related to the presence of a hole in the torus, which requires additional compatibility constraints around the hole for rigid foldability (Tachi, 2009). As a result, local folding compatibility at the vertices, although it takes the same form as force balance, is not sufficient to ensure global folding compatibility of the origami, thereby hindering the establishment of duality. Indeed, as noted by Tachi (2012), the compatibility condition around the hole can instead be interpreted as the moment balance of a rigid body occupying the hole. On a different note, if the framework is not associated with a polyhedron, such as triangulated origami patterns on a flat sheet (Chen and Santangelo, 2018), the duality cannot be established. This is because the boundary edges of the pattern are incident to only one face, and thus no dihedral angle can be defined along those edges. However, as long as the framework is homeomorphic to a sphere, the duality can still be established even for two-dimensional structures, as exemplified by the X-cross tensegrity and the collapsed tetrahedron discussed in Appendix E and shown in Fig. E.18. Although higher-order terms are required to analyze origami folding branches in the flat case (Chen and Santangelo, 2018), first-order foldability is sufficient for establishing the duality.

Fig. 3 illustrates the example of a truncated cubic tensegrity and its corresponding dual origami. The introduction of CAMs makes this equivalence explicit by reconciling the vanishing member forces in the tensegrity with the absence of panel bending in the origami, thereby bypassing the triangulation requirement. Although the truncated cubic tensegrity has been well understood (see Zhang et al. (2013) as well as Appendix B and Fig. A.8), the associated shaky origami is revealed here through the duality establishment. The infinitesimal mechanism of this truncated cubic origami is obtained from $\widetilde{\mathbf{B}}\mathbf{m} = \mathbf{0}$ and is shown in Fig. 3, bottom right. The duality theory can be numerically validated through checking $\mathbf{D}\mathbf{J}\mathbf{m} = \mathbf{0}$ and $\bar{\mathbf{J}}\mathbf{m} = \bar{\mathbf{0}}$. By varying the force densities of the rhombic tensegrities (including the tetrahedral, cubic, and dodecahedral forms), their configurations can be continuously modified (Zhang et al., 2013). Accordingly, the corresponding shaky origami arise naturally from the duality theory. These sphere-like origami are reported in Dang and Paulino (2026). In the remainder of the paper, we present in particular the tower-like configurations.

4. Duality of prismatic tensegrities and origami towers

By applying the proposed duality theory to the multilayer prismatic tensegrities (Appendix C and Figs. C.9–C.16), we construct a family of infinitesimally flexible origami towers, as illustrated in Fig. 4. Following Theorem 1, the infinitesimal mechanisms of the

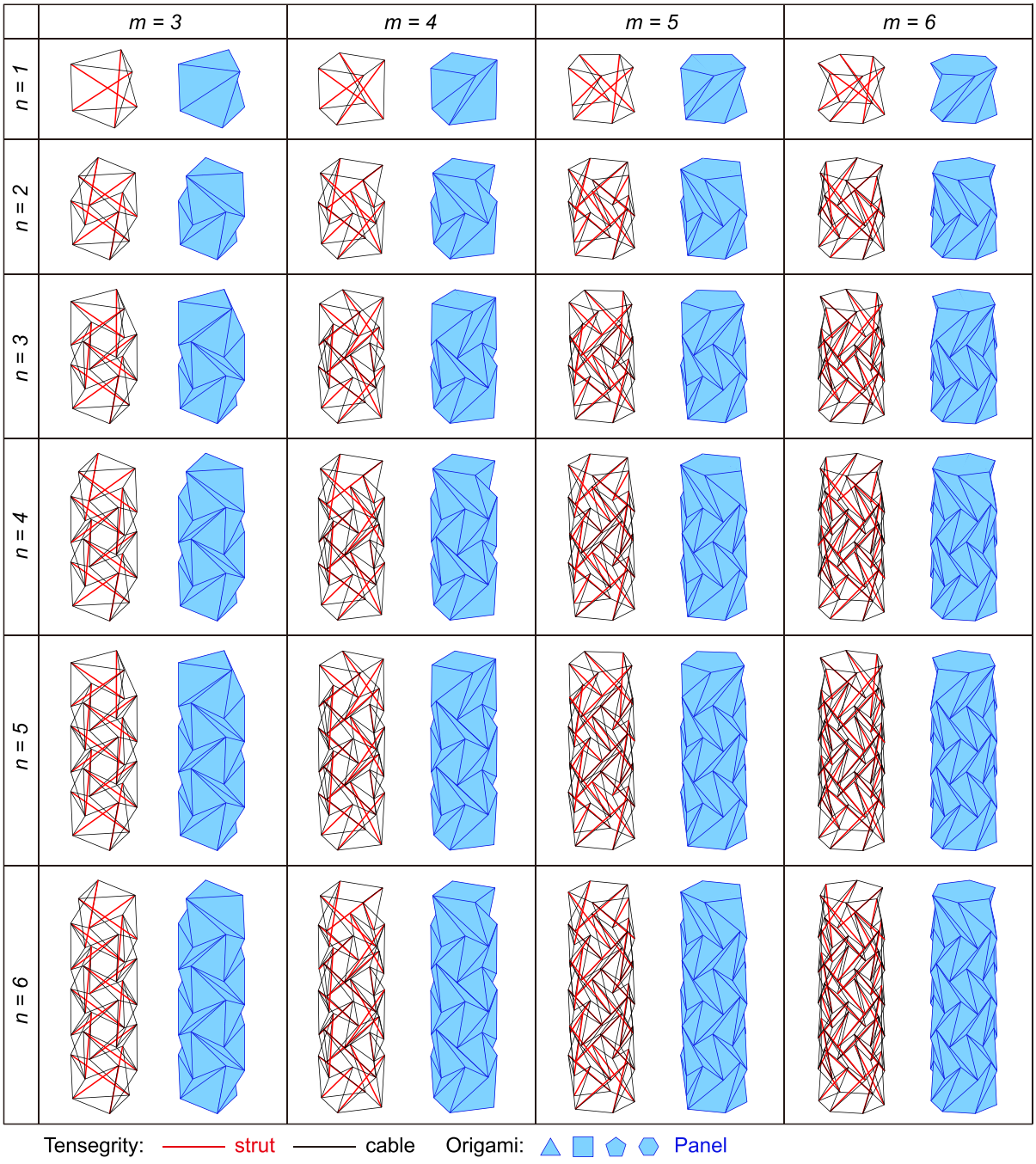

Fig. 4. Class-1 prismatic tensegrities and their dual origami towers for various numbers of struts per layer ($m = 3, 4, 5, 6$) and layer numbers ($n = 1, 2, \ldots, 6$). All configurations exhibit m-fold cyclic symmetry. For odd n, the structures possess flip symmetry, whereas for even n, they exhibit quasi-flip symmetry.

origami are obtained from the null space Null($\widetilde{\mathbf{B}}$). The matrix $\widetilde{\mathbf{B}}$ is assembled using the connectivity matrix $\mathbf{C}$ of the corresponding tensegrities (Nishimura, 2000), together with the connectivity $\overline{\mathbf{C}}$ and the Jacobian $\overline{\mathbf{J}}$ associated with the CAMs. As shown in Fig. 5, the deformed configurations preserve the dihedral symmetry (namely, cyclic symmetry combined with quasi-flip or flip symmetry), inherited from the dual configurations of the tensegrity and origami. It is noted that quasi-flip symmetry is associated with the reversed chirality of the top and bottom halves of origami towers with an even number of layers. That is, the crease directions alternate between clockwise and counterclockwise, but their sequence is reversed from the top down and from the bottom up. In other words, quasi-flip symmetry means that the two halves exhibit flip symmetry, with respect to a 180-degree rotation, only at the level of nodes, while the edges and faces do not coincide because of the reversed chirality. By contrast, origami towers with an odd

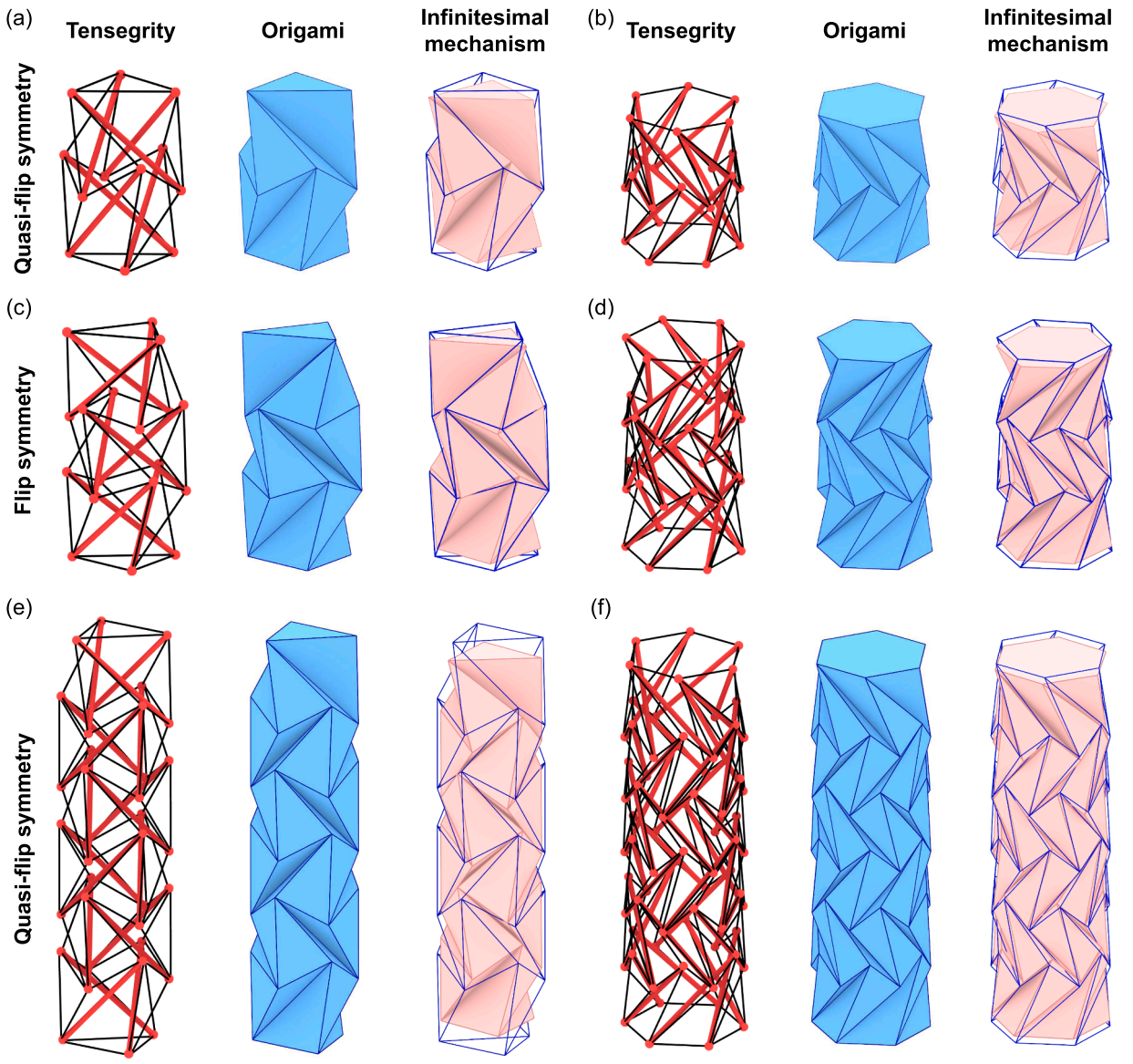

Fig. 5. Dual configurations of prismatic tensegrities and origami towers, together with the corresponding infinitesimal mechanisms, for various numbers of struts per layer ($m = 3, 6$) and layer numbers ($n = 2, 3, 6$). The blue lines indicate the undeformed outlines. (a) $m = 3$ and $n = 2$. (b) $m = 6$ and $n = 2$. (c) $m = 3$ and $n = 3$. (d) $m = 6$ and $n = 3$. (e) $m = 3$ and $n = 6$. (f) $m = 6$ and $n = 6$. The deformed structures show the same quasi-flip symmetry (for even $n = 2, 6$) or flip symmetry (for odd $n = 3$) as the dual configurations.

number of layers exhibit true flip symmetry, since their top and bottom halves have the same chirality. Interestingly, compression simulations reveal a loss of quasi-flip symmetry in certain two-layer configurations within the regime of finite deformations (see Section 5).

The prismatic tensegrities shown in Figs. 4 and 5 are characterized by discontinuous struts and continuous cables. That is, only one strut is connected to cables at each node. These class-1 tensegrities admit a single independent state of self-stress ($d_s = 1$), and correspondingly, the associated origami towers possess only one independent infinitesimal mechanism. However, Theorem 1 applies generally to arbitrary dimensions of the spaces $\mathbb{S}$ and $\mathbb{M}$. To illustrate this generality, we construct dual configurations with $d_s = d_m > 1$ by stacking the basic one-layer prismatic tensegrities and Kresling origami units. Fig. 6(a) shows these basic units that has either one independent state of self-stress ($s = 1$) or one independent infinitesimal mechanism ($m = 1$). As illustrated in Fig. 6(b)–(d), stacking these units increases the dimension of the spaces $\mathbb{S}$ or $\mathbb{M}$ by one for each additional layer ($s = m = 2, 3, 4$). The resulting stacked tensegrity towers are class-2 structures: each node shared by two adjacent layers is connected to one strut from each layer. The self-equilibrium of one layer does not influence that of the others, since each layer remains self-balanced, as in the one-layer configuration (Fig. 6(e)). The total internal force in the horizontal cables between two adjacent layers is obtained by superposing

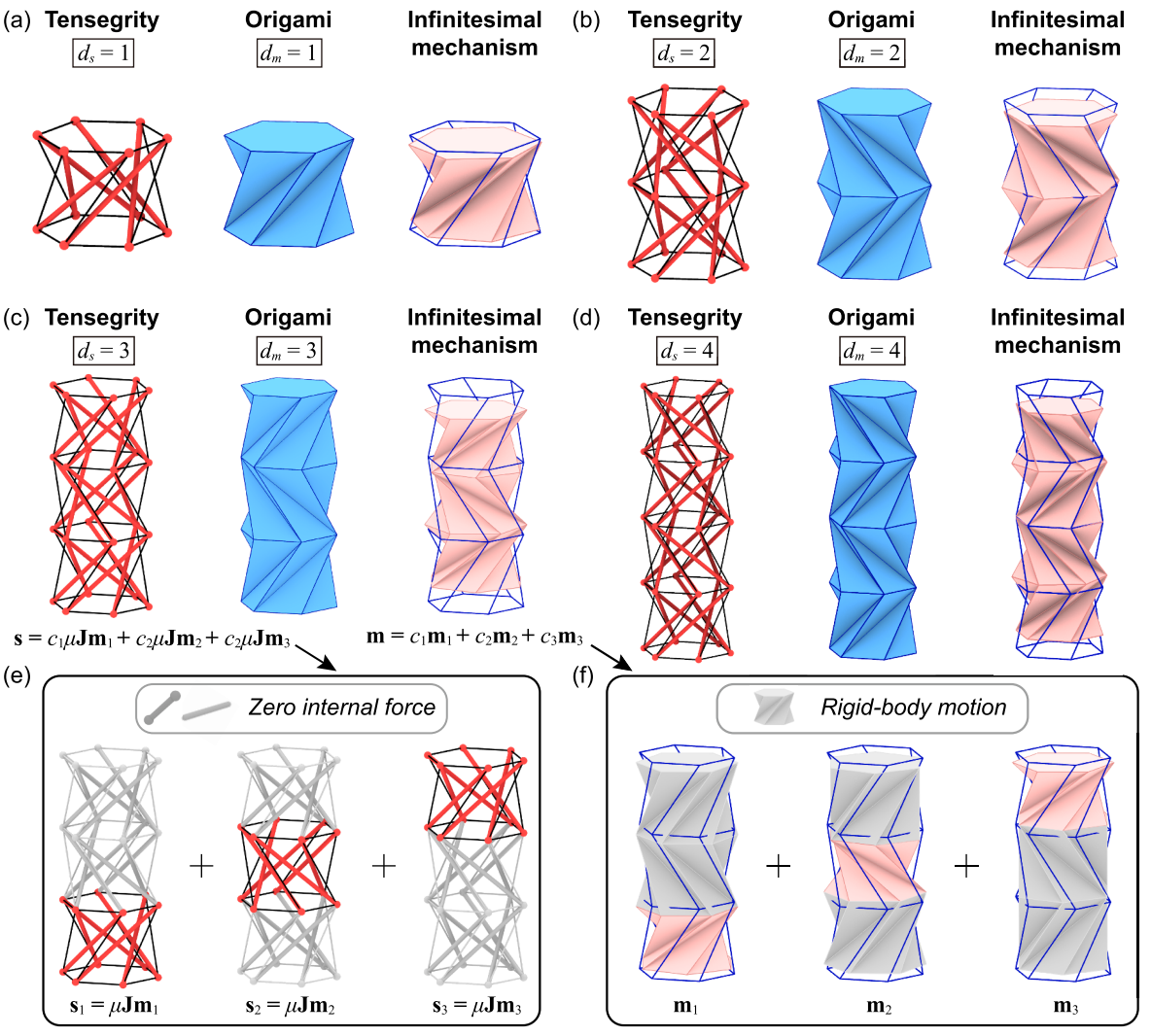

Fig. 6. Class-2 multilayer prismatic tensegrities, their dual stacked origami towers, and the corresponding infinitesimal mechanisms. The blue lines indicate the undeformed outlines. (a) The class-1 one-layer prismatic tensegrity and the shaky Kresling origami, which serve as the building blocks of the stacked configurations. These basic units admit one independent state of self-stress ($d_s = 1$) or one independent infinitesimal mechanism ($d_m = 1$). (b)–(d) The class-2 prismatic tensegrities and stacked origami towers, which possess multiple independent states of self-stress and multiple infinitesimal mechanisms, respectively ($d_s = d_m = 2, 3, 4$). The total internal force vector $\mathbf{s}$ is obtained by superposing (e) the individual self-stress states $\mathbf{s}_i = \mu\mathbf{J}\mathbf{m}_i$, each of which is dual to (f) the individual mechanism $\mathbf{m}_i$. Here, $\mathbf{J}$ denotes the Jacobian of the dihedral angles with respect to the nodal coordinates, μ is a nonzero scalar with units of N, and the coefficients c_i are dimensionless. Under the duality equivalence, the total mechanism displacement $\mathbf{m}$ is given by the superposition of the nodal displacements associated with the individual mechanisms $\mathbf{m}_i$.

the internal forces contributed by the two layers, whereas the internal forces in the remaining members coincide with those of the one-layer units. Accordingly, each layer of the stacked origami can deform independently, analogous to the behavior of a one-layer Kresling origami (Fig. 6(f)). Since the analytical expressions for the displacements of the individual Kresling units are derived in Appendix D, the overall deformation of the origami towers is obtained by the direct superposition of these individual displacements.

5. Finite deformation simulation of origami towers

We use a surrogate model to capture the finite deformations of the origami towers that are dual to class-1 prismatic tensegrities. As illustrated in Fig. 7(a), we focus on deformation modes with cyclic symmetry: nodes located at the same height remain on a circle, that may change its radius r_i, rotate by φ_i, and translate vertically by u_i. In this representation, each layer of an n-layer origami tower consists of two circles at distinct heights. Rigid-body motions are eliminated by fixing the bottom circle such that $u_{2n} = 0$ and $\varphi_{2n} = 0$. We assume that the deformation energy is stored in the side edges. The axial stiffness of member j is defined as $k_j = EA/\ell_j$, where ℓ_j is the undeformed member length and EA is the axial rigidity, assumed identical for all members. The total deformation energy

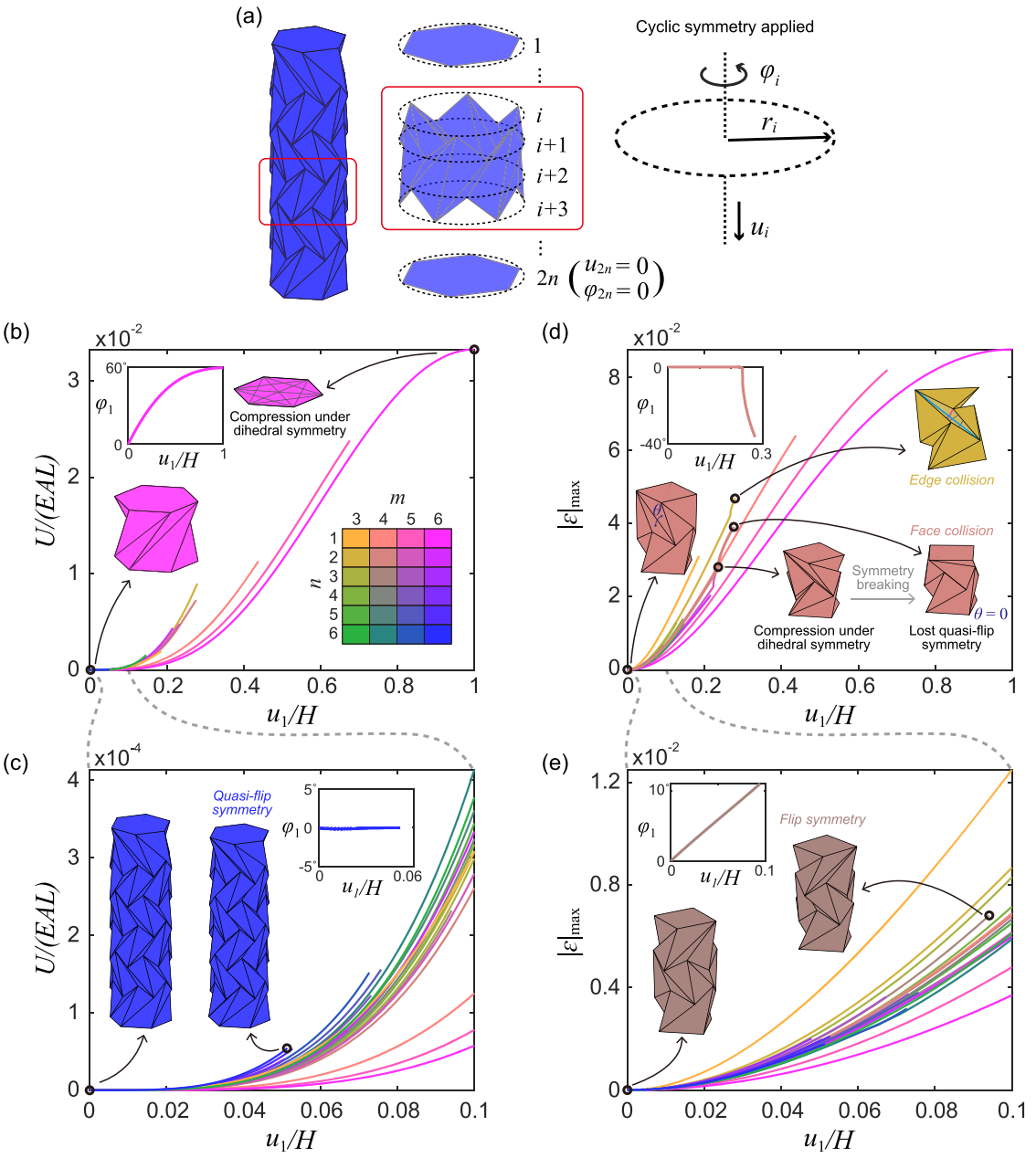

Fig. 7. Finite deformation simulation of origami towers. (a) The simulation is performed with cyclic symmetry: nodes located at the same height remain on a circle, that may change its radius r_i, rotate by φ_i, and translate vertically by u_i. Each layer of an n-layer origami tower consists of two circles at distinct heights. Rigid-body motions are eliminated by fixing the bottom circle such that $u_{2n} = 0$ and $\varphi_{2n} = 0$. (b) and (c) The nondimensionalized deformation energy $U/(EAL)$ and (d) and (e) the maximum member strain $|\varepsilon|_{\max}$ versus the nondimensionalized displacement u_1/H with varying numbers of layers and base polygon sides ($n = 1, 2, 3, 4, 5, 6$ and $m = 3, 4, 5, 6$). Here, EA is the axial rigidity, assumed identical for all members; L denotes the length of the undeformed valley crease in the bottom layer; H is the undeformed height of the origami tower. The insets plot the twist angles φ_1 between the two base polygons against u_1/H.

is then expressed as $U = \sum_{j=1}^{M} k_j(\ell_j' - \ell_j)^2/2$, where ℓ_j' denotes the deformed length of member j. The energy U is thus a function of the variables φ_i, u_i, and r_i. We consider compressive loading, such that the generalized constraint forces associated with rotational and radial variations vanish. Based on the principle of minimum potential energy, we minimize U under incremental increases of u_1 from zero until panel contact occurs (i.e., when a dihedral angle reduces to zero). An exception arises for the two-layer, square-based configuration ($m = 4$ and $n = 2$), in which edge collision is detected instead (see Fig. 7(d)). At each loading step, specified by u_1, we solve for the free variables φ_i and r_i. In this manner, we obtain the deformation paths of the origami towers, including

the nondimensionalized deformation energy $U/(EAL)$ and the maximum member strain $|\varepsilon|_{\max}$. Here, L denotes the length of the undeformed valley crease in the bottom layer. The optimization is performed using the function *fmincon* in the software matlab R2023b.

We employ the proposed reduced-order model to simulate the finite compressive deformations of origami towers with varying numbers of layers and base polygon sides ($n = 1, 2, 3, 4, 5, 6$ and $m = 3, 4, 5, 6$). These configurations are illustrated in Fig. 4. The corresponding simulation results are shown in Fig. 7(b) and (c) for the nondimensionalized deformation energy $U/(EAL)$, and in Fig. 7(d) and (e) for the maximum member strain $|\varepsilon|_{\max}$. We observe that the initial slope of the $|\varepsilon|_{\max}$ curves is zero, thereby confirming the presence of infinitesimal mechanisms, as predicted by the duality theory. Moreover, although only cyclic symmetry is imposed in the simulations, quasi-flip symmetry (Fig. 7(c)) or flip symmetry (Fig. 7(e)) is generally preserved during deformation, contributing to the overall dihedral symmetry of the deformed configurations. However, as compression increases, symmetry breaking is observed in two-layer towers ($m = 3, 4, 5$ and $n = 2$). This manifests as a loss of quasi-flip symmetry and the emergence of a nonzero twist φ_1 of the base polygons, which also leads to non-smooth variations in the $|\varepsilon|_{\max}$ curves (Fig. 7(d)). The symmetry breaking of origami towers warrants further investigation in future work.

6. Concluding remarks

We present a general duality theory that establishes the equivalence between the self-stress of tensegrities and the folding mechanisms of origami. This duality is revealed through a unified pin-jointed framework representation incorporating constrained auxiliary members. The constrained auxiliary members are characterized by zero internal force in the tensegrity and by zero extension and zero dihedral-angle variation in the origami. These properties lead to an equivalent geometric interpretation of the pin-jointed framework: the tensegrity corresponds to the 1-skeleton of a polyhedron, while the origami corresponds to the 2-skeleton of the same polyhedron. The duality fundamentally arises from the geometry of the underlying polyhedron, which must be nonconvex and homeomorphic to a sphere. The nonconvexity enables the existence of infinitesimal flexibility in the origami, consistent with Cauchy's rigidity theorem. The homeomorphism to a sphere ensures the coexistence of self-equilibrium in the tensegrity through the specific Euler characteristic $\chi = 2$. We present a variety of dual configurations with spherical and prismatic geometries. Building on prior knowledge for tensegrities, the duality theory reveals the corresponding shaky origami structures. Furthermore, as demonstrated by Dang and Paulino (2026), the duality relationship can be substantially extended via linear transformations under the same connectivity, while preserving the shakiness, self-equilibrium, and super-stability from regular to irregular configurations.

CRediT authorship contribution statement

Xiangxin Dang: Writing – review & editing, Writing – original draft, Visualization, Validation, Software, Methodology, Investigation, Formal analysis, Data curation, Conceptualization; **Glaucio H. Paulino:** Writing – review & editing, Validation, Supervision, Resources, Project administration, Methodology, Funding acquisition, Conceptualization.

Declaration of competing interest

The authors declare that they have no known competing financial interests or personal relationships that could have appeared to influence the work reported in this paper.

Acknowledgments

This material is based upon work supported by the National Science Foundation (NSF) under Award no. 2323276; the Princeton Catalysis Initiative (PCI), Princeton University; and the Eric and Wendy Schmidt Transformative Technology Fund, Princeton University. Any opinions, findings and conclusions or recommendations expressed in this paper are those of the authors and do not necessarily reflect the views of the sponsors.

Data availability

Data will be made available on request.

Appendix A. Super-stability definition and conditions (Connelly, 2002; Zhang and Ohsaki, 2015)

We take the definition of super-stability from Zhang and Ohsaki (2015): If a prestressed free-standing pin-jointed framework is always stable in the state of self-equilibrium, in the sense of having locally strict minimum of the total potential energy, irrespective of material properties as well as level of prestresses (i.e., signs of the prestresses should not be changed, while the magnitude of the prestresses can be arbitrarily scaled in proportion satisfying the self-equilibrium equations), then it is super-stable. If the following three conditions are all satisfied, then the three-dimensional free-standing pin-jointed framework is super stable:

(a) Rank of the geometry matrix **G** is equal to six;
(b) The force density matrix **E** has the minimum necessary rank deficiency four;

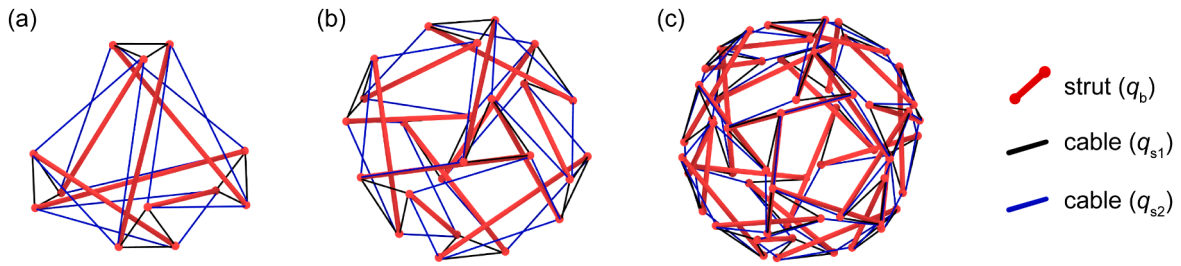

Fig. A.8. Rhombic truncated regular polyhedral (TRP) tensegrities. (a) The truncated tetrahedral, (b) the cubic, and (c) the dodecahedral configurations.

(c) The force density matrix **E** is positive semi-definite.

The conditions (a) and (c) are also necessary for super-stability. Moreover, we note that the condition (a) is generally satisfied if and only if all the member directions of the tensegrity are not incident with a *conic at infinity*, as stated in the following lemma:

Lemma 2. *In the three-dimensional case, rank of the geometric matrix* **G** *is equal to six, if and only if the member directions do not lie on the same conic at infinity.*

Here, a conic at infinity is defined by a nonzero symmetric matrix **N** such that every point **u** on this conic satisfies $\mathbf{u}^{\mathrm{T}}\mathbf{N}\mathbf{u} = 0$. By orthogonally diagonalizing the symmetric matrix **N**, this definition can be expressed as $\lambda_1 u^2 + \lambda_2 v^2 + \lambda_3 w^2 = 0$ under a proper Cartesian coordinate system $O - uvw$, where λ_i $(i = 1, 2, 3)$ are the three real eigenvalues of **N**. When all eigenvalues are nonzero and not of the same sign, this equation represents a double cone extending infinitely in both directions from the apex, rather than degenerating into a point or a pair of lines. We observe that, for both the rhombic TRP tensegrities (see examples in Fig. A.8) and the single- or multilayer prismatic tensegrities (see examples in Figs. C.9–C.16), the member directions do not lie on a common conic at infinity. Therefore, condition (a) for super-stability is satisfied.

Appendix B. Equilibrium and super-stability of rhombic TRP tensegrity (Zhang et al., 2013)

We refer to Zhang et al. (2013) for the connectivity diagram that determines the connectivity matrix of rhombic TRP tensegrities. A rhombic TRP tensegrity is self-equilibrium and super-stable *if and only if* the force densities satisfy:

$$\begin{aligned} -\frac{q_{s1}}{q_b} &= Q_1, \\ -\frac{q_{s2}}{q_b} &= \frac{\sqrt{\left(3Q_1^2 - 4Q_1 + 1\right)^2 + 2Q_1\left(6Q_1^2 - 7Q_1 + 2\right)\left(1 - \cos\frac{2\pi}{b}\right)} - \left(3Q_1^2 - 4Q_1 + 1\right)}{2\left(2Q_1 - 1\right)\left(1 - \cos\frac{2\pi}{b}\right)}, \end{aligned} \tag{B.1}$$

for $Q_1 > 1/2$ and $b = 3, 4, 5$. When $b = 3$, the tensegrity takes a tetrahedral form (Fig. A.8(a)); when $b = 4$, a cubic/octahedral form (Fig. A.8(b)); and when $b = 5$, a dodecahedral/icosahedral form (Fig. A.8(c)).

Appendix C. Equilibrium and super-stability of prismatic tensegrity

C.1. Equilibrium

We refer to Nishimura (2000) for the connectivity diagram that determines the connectivity matrix of prismatic tensegrities presented in this appendix. The closed-form solutions for the one- and two-layer prismatic tensegrities are taken from the work of Nishimura (2000), who also established the characteristic equation governing equilibrium for n-layer ($n \geq 3$) configurations. Building on this development, we further derive closed-form solutions for the n-layer ($n \geq 3$) case. In this section, a multilayer prismatic tensegrity is assumed to have uniform strut number m, height H, radius r, and overlap ratio γ across all layers. The interior layers are further assumed to share a uniform twist angle, denoted by $\alpha^\star$ (applicable when $n \geq 3$), whereas the twist angle of the boundary layers is denoted by α (applicable when $n \geq 1$).

C.1.1. One-layer configurations (Nishimura, 2000)

The geometric symmetry of prismatic tensegrities plays a crucial role in simplifying their equilibrium conditions and facilitating the derivation of closed-form solutions. As shown in Fig. C.9, the one-layer prismatic tensegrity exhibits m-fold rotation symmetry and m two-fold rotation symmetries. Together, these symmetries constitute the dihedral symmetry of the structure. This symmetry description was adopted by Zhang et al. (2009a,b), Zhang and Ohsaki (2015). Nishimura (2000) referred to the m-fold rotational

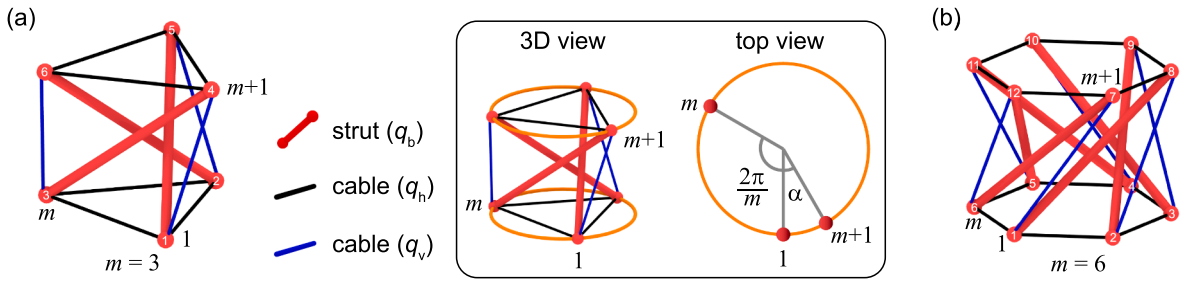

Fig. C.9. One-layer prismatic tensegrities with (a) triangular and (b) hexagonal base polygons. In general, for base polygons with m sides, the corresponding twist angle is given by $\alpha = \pi/2 - \pi/m$.

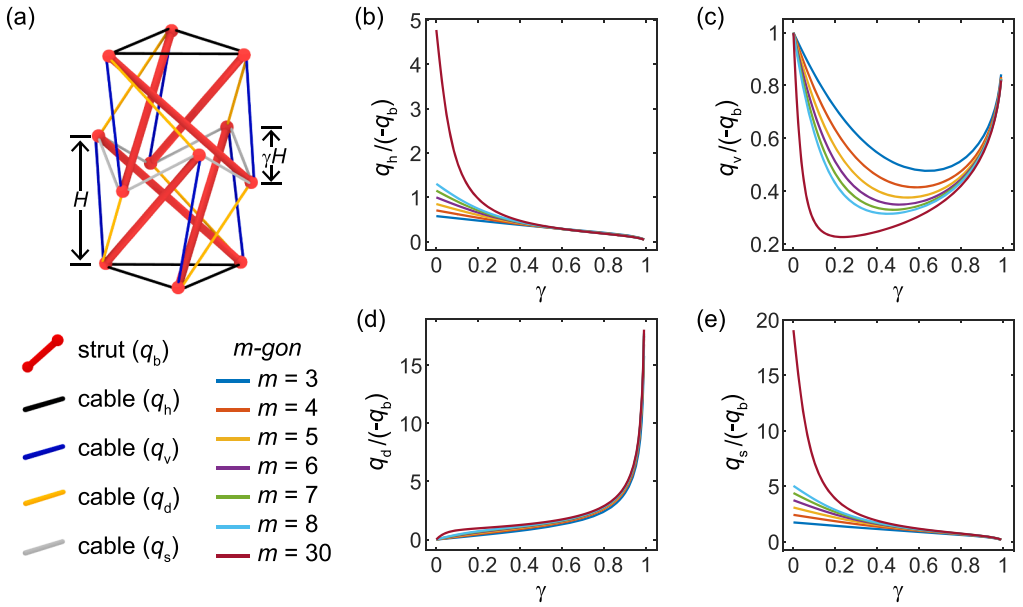

Fig. C.10. Two-layer prismatic tensegrities. (a) Configuration with triangular base polygons. (b)–(e) Force-density ratios $q_h/(-q_b)$, $q_v/(-q_b)$, $q_d/(-q_b)$, and $q_s/(-q_b)$ plotted against the overlap ratio γ for base polygons with m sides ($m = 3, 4, 5, 6, 7, 8, 30$).

symmetry as *cyclic symmetry* and the two-fold rotational symmetry as *flip symmetry*. The equilibrium condition for the one-layer prismatic tensegrity is given by

$$\alpha = \frac{\pi}{2} - \frac{\pi}{m}. \tag{C.1}$$

Under the condition in Eq. (C.1), the corresponding force densities satisfy

$$\begin{aligned} \frac{q_h}{-q_b} &= \frac{1}{2\sin\frac{\pi}{m}}, \\ \frac{q_v}{-q_b} &= 1. \end{aligned} \tag{C.2}$$

Here, q_b denotes the force density of the struts; q_h and q_v denote the force densities of the two different types of cables, namely horizontal cables and vertical cables, respectively (see Fig. C.9(a)). We note that the term *vertical cables*, following Nishimura (2000), does not imply strict alignment with the vertical direction. Rather, it is used to distinguish their geometric configuration from that of the horizontal cables.

C.1.2. Two-layer configurations (Nishimura, 2000)

As shown in Fig. C.10(a), the two-layer prismatic tensegrity exhibits m-fold cyclic symmetry and m quasi-flip symmetries. Here, the *quasi-flip symmetry*, following the description of Nishimura (2000), is associated to a two-fold rotation that coincides nodes but

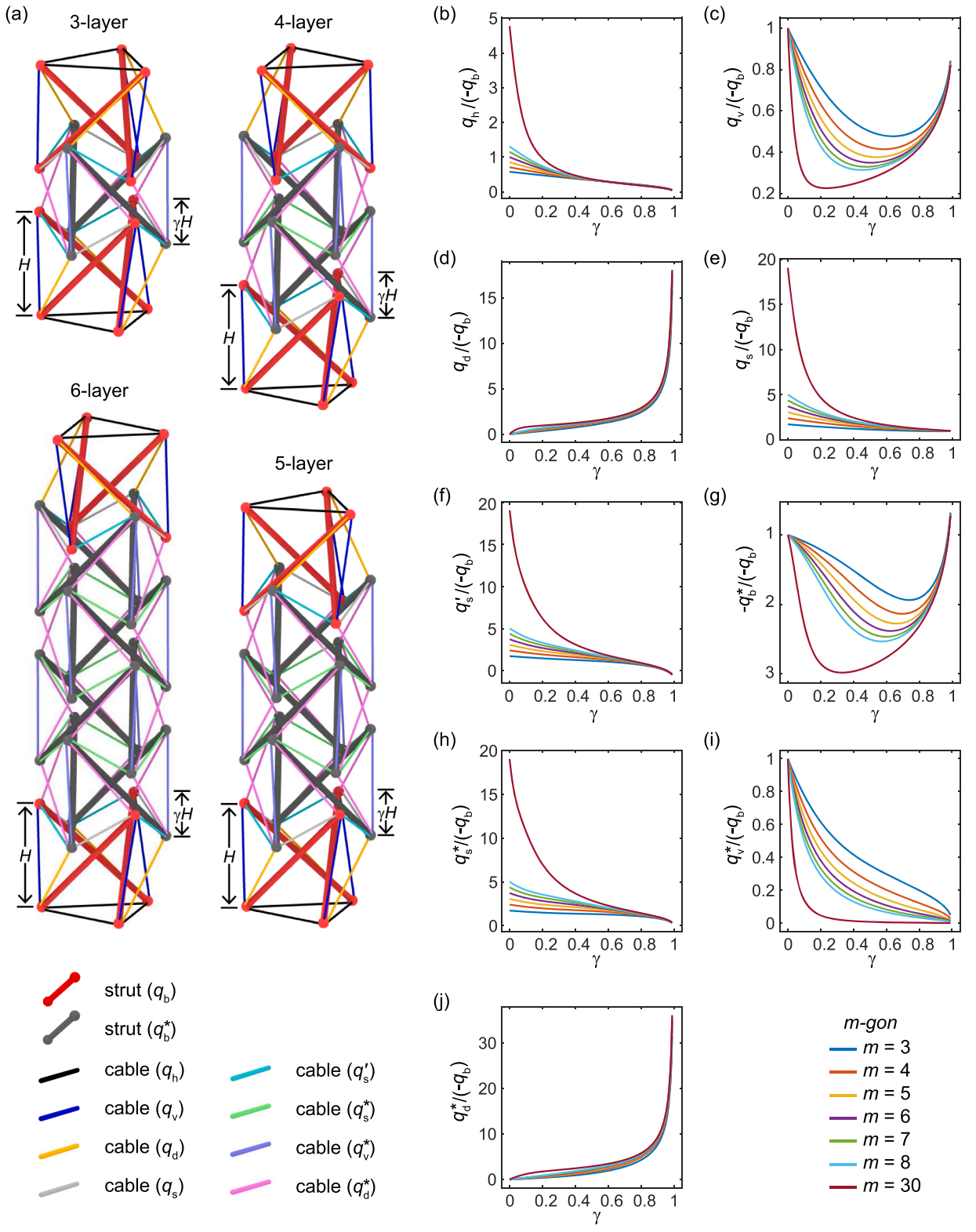

Fig. C.11. Multilayer prismatic tensegrities. (a) Configurations with triangular base polygons. (b)–(j) Force-density ratios $q_h/(-q_b)$, $q_v/(-q_b)$, $q_d/(-q_b)$, $q_s/(-q_b)$, $q_s'/(-q_b)$, $-q_b^*/(-q_b)$, $q_s^*/(-q_b)$, $q_v^*/(-q_b)$, $q_d^*/(-q_b)$ plotted against the overlap ratio γ for base polygons with m sides (m = 3, 4, 5, 6, 7, 8, 30).

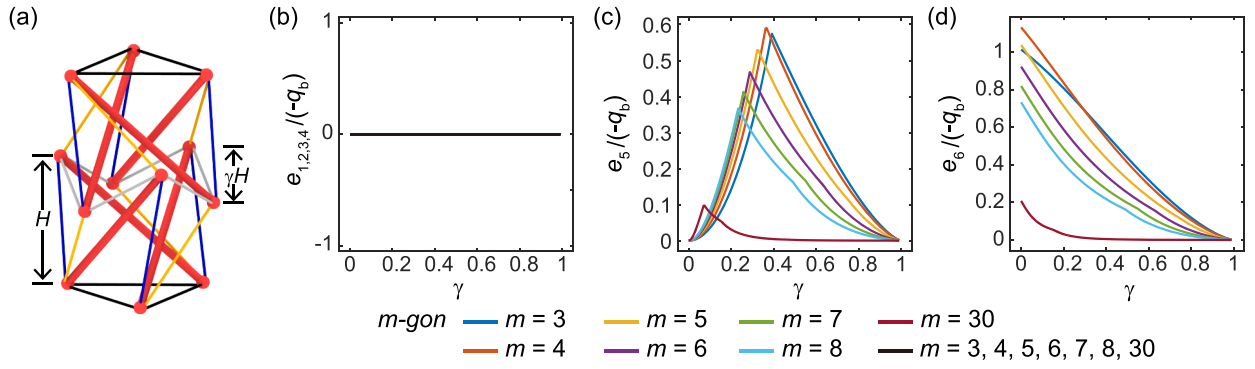

Fig. C.12. Six smallest eigenvalues e_i $(i = 1, 2, \ldots, 6)$ of the force density matrix **E** for two-layer prismatic tensegrities. The eigenvalues are computed for overlap ratios $\gamma \in (0, 1)$ and for base polygons with m sides $(m = 3, 4, 5, 6, 7, 8, 30)$, and are nondimensionalized by the magnitude of the strut force density, $-q_b$. (a) Configuration with triangular base polygons. (b)–(d) $e_i/(-q_b)$ $(i = 1, 2, 3, 4, 5, 6)$ versus γ.

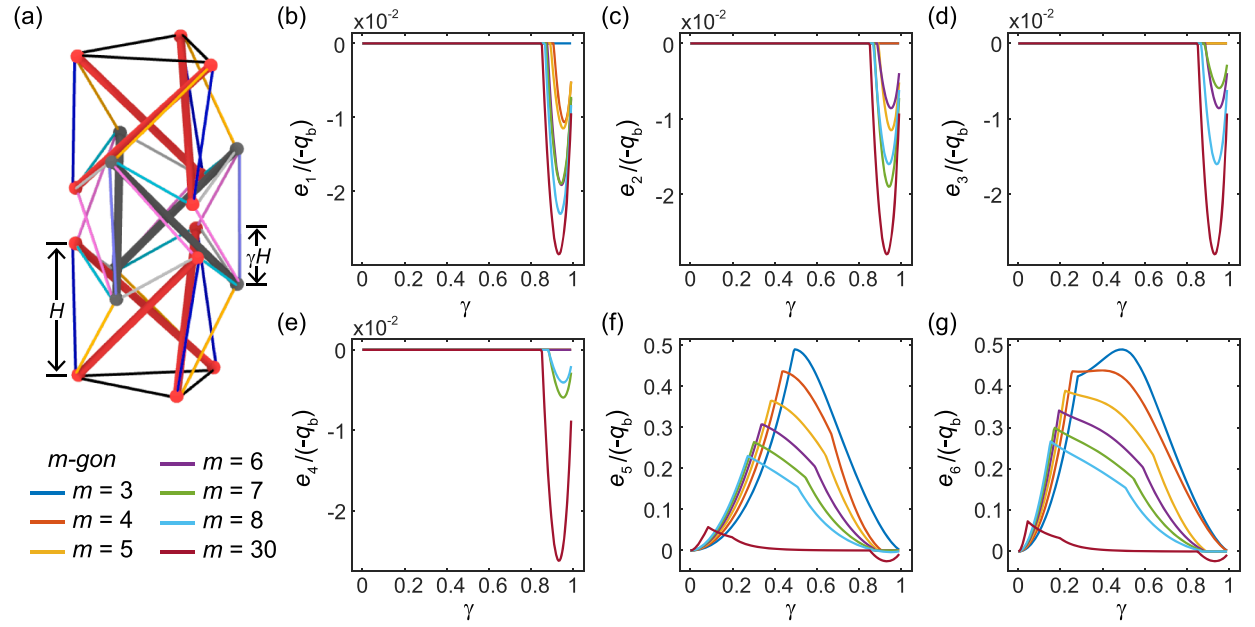

Fig. C.13. Six smallest eigenvalues e_i $(i = 1, 2, \ldots, 6)$ of the force density matrix **E** for three-layer prismatic tensegrities. The eigenvalues are computed for overlap ratios $\gamma \in (0, 1)$ and for base polygons with m sides $(m = 3, 4, 5, 6, 7, 8, 30)$, and are nondimensionalized by the magnitude of the strut force density, $-q_b$. (a) Configuration with triangular base polygons. (b)–(g) $e_i/(-q_b)$ $(i = 1, 2, 3, 4, 5, 6)$ versus γ.

reverses chirality of members. The equilibrium condition for the two-layer prismatic tensegrity is given by

$$\cos\left(\frac{\pi}{m}+\alpha\right)=\frac{\gamma\left[1-(1-\gamma)\cos\frac{\pi}{m}\right]}{2(1-\gamma)\left(1-\cos\frac{\pi}{m}\right)+\gamma^2}. \tag{C.3}$$

Under the condition in Eq. (C.3), the corresponding force densities satisfy

$$\frac{q_h}{-q_b}=\frac{1}{2D\sin\frac{\pi}{m}}\left[1-(1-\gamma)\cos\frac{\pi}{m}-\gamma\cos\left(\frac{\pi}{m}+\alpha\right)\right],$$

$$\frac{q_v}{-q_b}=\frac{1}{D}\left[\sin\left(\frac{\pi}{m}+\alpha\right)-(1-\gamma)\sin\left(\frac{2\pi}{m}+\alpha\right)\right],$$

$$\frac{q_d}{-q_b}=\frac{1}{D}\left[\sin\left(\frac{2\pi}{m}+\alpha\right)-\sin\alpha\right],$$

$$\frac{q_s}{-q_b}=\frac{1}{4D\sin\frac{\pi}{m}\left(1-\cos\frac{\pi}{m}\right)}\left\{2\left(1-\cos\frac{2\pi}{m}\right)+(1-\gamma)\left(\cos\frac{3\pi}{m}-\cos\frac{\pi}{m}\right)\right.$$

$$+\gamma\left[\cos\left(\frac{3\pi}{m}+\alpha\right)-2\cos\left(\frac{\pi}{m}+\alpha\right)+\cos\left(\frac{\pi}{m}-\alpha\right)\right]\Big\}, \tag{C.4}$$

with

$$D=\sin\left(\frac{\pi}{m}+\alpha\right)-(1-\gamma)\sin\alpha. \tag{C.5}$$

Here, q_{b} denotes the force density of the struts; q_{h}, q_{v}, q_{d}, and q_{s} denote the force densities of the four different types of cables, namely horizontal cables, vertical cables, diagonal cables, and saddle cables, respectively (see Fig. C.10(a)). These force-density ratios vary with the overlap ratio γ and per-layer strut number m, as plotted in Fig. C.10(b)–(e). We note that Eqs. (C.3)–(C.5) have been

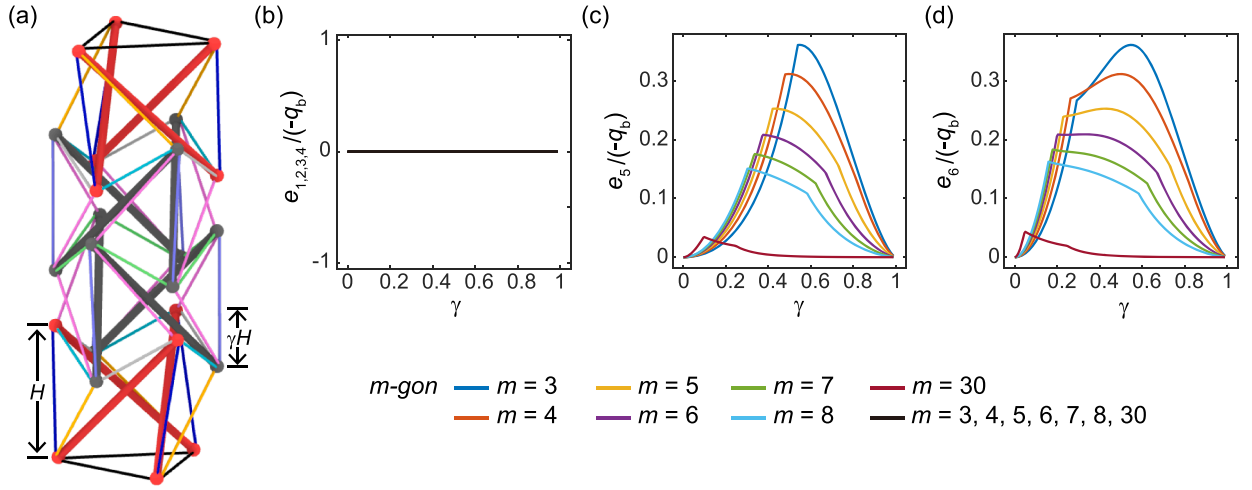

Fig. C.14. Six smallest eigenvalues e_i $(i=1,2,\ldots,6)$ of the force density matrix $\mathbf{E}$ for four-layer prismatic tensegrities. The eigenvalues are computed for overlap ratios $\gamma\in(0,1)$ and for base polygons with m sides $(m=3,4,5,6,7,8,30)$, and are nondimensionalized by the magnitude of the strut force density, $-q_{\mathrm{b}}$. (a) Configuration with triangular base polygons. (b)–(d) $e_i/(-q_{\mathrm{b}})$ $(i=1,2,3,4,5,6)$ versus γ.

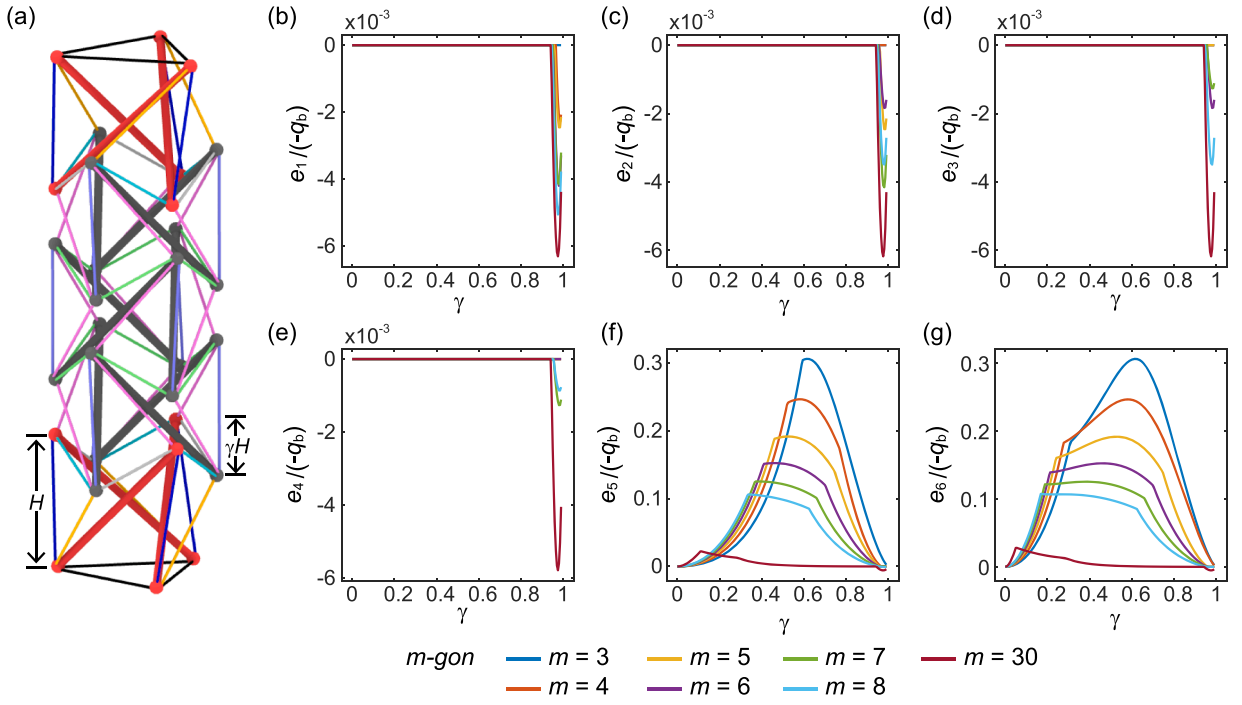

Fig. C.15. Six smallest eigenvalues e_i $(i=1,2,\ldots,6)$ of the force density matrix $\mathbf{E}$ for five-layer prismatic tensegrities. The eigenvalues are computed for overlap ratios $\gamma\in(0,1)$ and for base polygons with m sides $(m=3,4,5,6,7,8,30)$, and are nondimensionalized by the magnitude of the strut force density, $-q_{\mathrm{b}}$. (a) Configuration with triangular base polygons. (b)–(g) $e_i/(-q_{\mathrm{b}})$ $(i=1,2,3,4,5,6)$ versus γ.

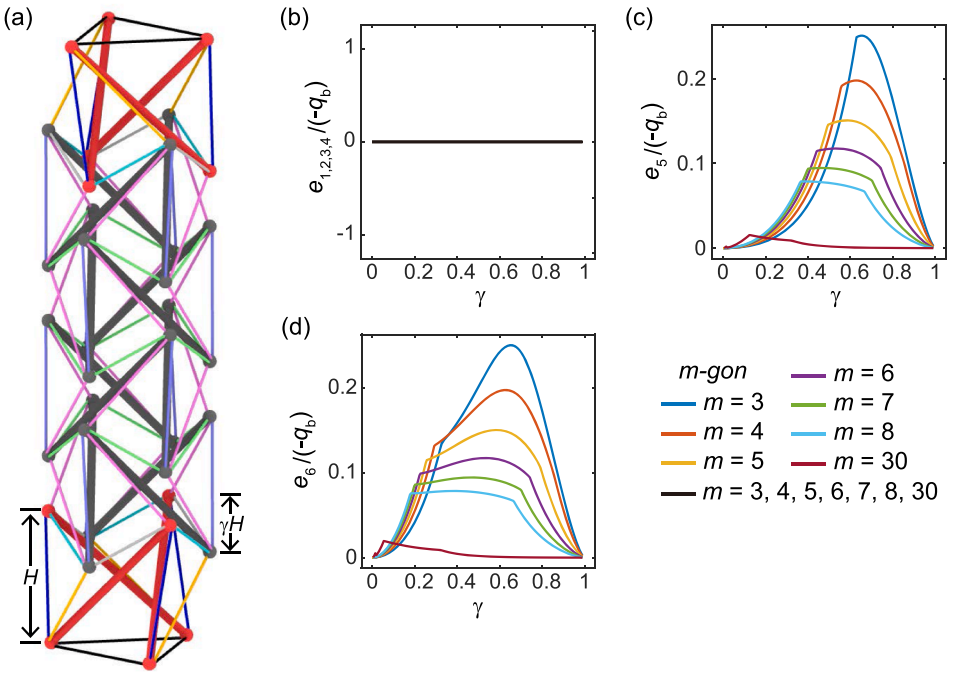

Fig. C.16. Six smallest eigenvalues e_i $(i = 1, 2, \ldots, 6)$ of the force density matrix $\mathbf{E}$ for six-layer prismatic tensegrities. The eigenvalues are computed for overlap ratios $\gamma \in (0, 1)$ and for base polygons with m sides $(m = 3, 4, 5, 6, 7, 8, 30)$, and are nondimensionalized by the magnitude of the strut force density, $-q_b$. (a) Configuration with triangular base polygons. (b)–(d) $e_i/(-q_b)$ $(i = 1, 2, 3, 4, 5, 6)$ versus γ.

simplified by assuming that the boundary nodes on the base polygons and the interior nodes share the same radius. When the radii differ, minor modifications can be introduced to obtain the corresponding expressions, as detailed by Nishimura (2000). Additionally, Eqs. (C.4) and (C.5) give the closed-form solutions of force densities, with the bar force density taken as the reference. If instead the horizontal cable is chosen as the reference, the force-density ratios become

$$\begin{aligned}
\frac{q_b}{q_h} &= -\frac{2\sin\frac{\pi}{m}}{D'}\left[\sin\left(\frac{\pi}{m}+\alpha\right)-(1-\gamma)\sin\alpha\right],\\
\frac{q_v}{q_h} &= 2\left(\sin\frac{\pi}{m}\right)\left[\sin\left(\frac{\pi}{m}+\alpha\right)-(1-\gamma)\sin\left(\frac{2\pi}{m}+\alpha\right)\right],\\
\frac{q_d}{q_h} &= 2\left(\sin\frac{\pi}{m}\right)\left[\sin\left(\frac{2\pi}{m}+\alpha\right)-\sin\alpha\right],\\
\frac{q_s}{q_h} &= 4\cos^2\frac{\pi}{2m},
\end{aligned} \tag{C.6}$$

with

$$D' = 1-(1-\gamma)\cos\frac{\pi}{m}-\gamma\cos\left(\frac{\pi}{m}+\alpha\right). \tag{C.7}$$

C.1.3. n-layer ($n \geq 3$) configurations

The multilayer prismatic tensegrities are assumed to exhibit m-fold cyclic symmetry together with m flip or quasi-flip symmetries. When the number of layers is even $(n = 4, 6, 8, \ldots)$, the structures possess quasi-flip symmetries, whereas for an odd number of layers $(n = 3, 5, 7, \ldots)$ they exhibit flip symmetries. Fig. C.11(a) illustrates several examples of the multilayer prismatic tensegrities with triangular bases $(m = 3)$. In the subsequent formulation, the tensegrities are assumed to have uniform force densities $q_b^\star$, $q_s^\star$, $q_v^\star$, $q_d^\star$ across all interior layers. This assumption, together with the uniform geometric features (regarding the strut number, height, radius, and overlap ratio, etc), leads to the following equilibrium condition (Nishimura, 2000)

$$\begin{aligned}
\cos\left(\frac{\pi}{m}+\alpha\right) &= \frac{\gamma\left[1-(1-\gamma)\cos\frac{\pi}{m}\right]}{2(1-\gamma)\left(1-\cos\frac{\pi}{m}\right)+\gamma^2},\\
\cos\left(\frac{\pi}{m}+\alpha^\star\right) &= \frac{\gamma\left[1-(1-\gamma)\cos\frac{\pi}{m}\right]}{(1-\gamma)\left(1-\cos\frac{\pi}{m}\right)+\gamma^2}.
\end{aligned} \tag{C.8}$$

Under the condition in Eq. (C.8), we derive the following force density ratios

$$\begin{aligned}
\frac{q_{\mathrm{b}}}{q_{\mathrm{h}}} &= -\frac{2\sin\frac{\pi}{m}}{D}\left[\sin\left(\frac{\pi}{m}+\alpha\right)-(1-\gamma)\sin\alpha\right],\\
\frac{q_{\mathrm{v}}}{q_{\mathrm{h}}} &= \frac{2\sin\frac{\pi}{m}}{D}\left[\sin\left(\frac{\pi}{m}+\alpha\right)-(1-\gamma)\sin\left(\alpha+\frac{2\pi}{m}\right)\right],\\
\frac{q_{\mathrm{d}}}{q_{\mathrm{h}}} &= \frac{4\gamma\cos^2\frac{\pi}{2m}}{1-\gamma},\\
\frac{q_{\mathrm{s}}}{q_{\mathrm{h}}} &= \frac{2\cos^2\frac{\pi}{2m}(4B+2\gamma-3\gamma^2)}{2B-\gamma^2}+\frac{\gamma\cot\frac{\pi}{2m}\sin\left(\frac{\pi}{m}+\alpha\right)}{1-\gamma}-\frac{4BC\gamma\sin\left(\frac{\alpha^\star}{2}+\frac{\pi}{m}\right)}{(2B-\gamma^2)(B-\gamma^2)},\\
\frac{q'_{\mathrm{s}}}{q_{\mathrm{h}}} &= \frac{2\cos^2\frac{\pi}{2m}(4B+2\gamma-3\gamma^2)}{2B-\gamma^2}-\frac{\gamma\cot\frac{\pi}{2m}\sin\left(\frac{\pi}{m}+\alpha\right)}{1-\gamma}-\frac{4BC\gamma\sin\frac{\alpha^\star}{2}}{(2B-\gamma^2)(B-\gamma^2)},\\
\frac{q^\star_{\mathrm{b}}}{q_{\mathrm{h}}} &= -\frac{4AB^2C}{(1-\gamma)(2B-\gamma^2)(B-\gamma^2)},\\
\frac{q^\star_{\mathrm{s}}}{q_{\mathrm{h}}} &= \frac{4B^2C^2}{(1-\gamma)(2B-\gamma^2)(B-\gamma^2)},\\
\frac{q^\star_{\mathrm{v}}}{q_{\mathrm{h}}} &= \frac{4B^2C(A-2\gamma C)}{(1-\gamma)(2B-\gamma^2)(B-\gamma^2)},\\
\frac{q^\star_{\mathrm{d}}}{q_{\mathrm{h}}} &= \frac{4B\gamma\sin^2\frac{\pi}{m}}{(2B-\gamma^2)(B-\gamma^2)},
\end{aligned} \tag{C.9}$$

with

$$\begin{aligned}
A &= \sin\left(\frac{\pi}{m}+\frac{\alpha^\star}{2}\right)-\sin\frac{\alpha^\star}{2}+2\gamma\sin\frac{\alpha^\star}{2},\\
B &= \gamma^2+(1-\gamma)\left(1-\cos\frac{\pi}{m}\right),\\
C &= \sin\left(\frac{\pi}{m}+\frac{\alpha^\star}{2}\right)+\sin\frac{\alpha^\star}{2},\\
D &= 1-\left[\gamma\cos\left(\frac{\pi}{m}+\alpha\right)+(1-\gamma)\cos\frac{\pi}{m}\right].
\end{aligned} \tag{C.10}$$

Here, q_{b}, q_{h}, q_{v}, and q_{d} are associated with the boundary (i.e., first and last) layers; they denote the force densities of struts, horizontal cables, vertical cables, and diagonal cables, respectively (see Fig. C.11(a)). At the interfaces between the boundary layers and the interior layers, two types of saddle cables are present, denoted by q_{s} and q'_{s}. For the interior layers, the force densities of struts, saddle cables, vertical cables, and diagonal cables are denoted by $q^\star_{\mathrm{b}}$, $q^\star_{\mathrm{s}}$, $q^\star_{\mathrm{v}}$, and $q^\star_{\mathrm{d}}$, respectively. These force-density ratios vary with the overlap ratio γ and the per-layer strut number m, as plotted in Fig. C.11(b)–(j). We note that Eqs. (C.9) and (C.10) are derived here from the characteristic equations established by Nishimura (2000), which were solved only numerically in that previous work.

C.2. Super-stability

The one-layer prismatic tensegrities are always super-stable, regardless of the number of struts m. We note that the prismatic tensegrities considered here share the feature that the horizontal cables connect adjacent nodes. A more general class of one-layer prismatic tensegrities with dihedral symmetry, where the horizontal cables may span beyond neighboring nodes, was investigated by Connelly and Terrell (1995), Zhang et al. (2009a,b), Zhang and Ohsaki (2015). The super-stability condition established therein is precisely that the horizontal cables connect adjacent nodes. Moreover, we observe that connections extending beyond adjacent nodes preclude a duality interpretation, as no flat, non-intersecting faces can be constructed for the corresponding dual origami under such connections.

We further investigate the super-stability of prismatic tensegrities with two or more layers. As discussed in Appendix A, we only need to check the conditions (b) and (c). These two conditions, that the force density matrix $\mathbf{E}$ is of rank deficiency four and positive semi-definite, are equivalent to requiring that $\mathbf{E}$ has exactly four zero eigenvalues and all the other eigenvalues are positive. Thus, we compute the six smallest eigenvalues e_i ($i = 1, 2, \ldots, 6$) of $\mathbf{E}$ for various multilayer prismatic tensegrities, with layer number $n = 2, 3, 4, 5, 6$ and per-layer strut number $m = 3, 4, 5, 6, 7, 8, 30$. The computations are carried out using the function *eigs* in the software Matlab R2023b, and the results are plotted in Figs. C.12–C.16. From the presented data, we make the following observations. The force density matrix $\mathbf{E}$ may fail to be positive semi-definite for prismatic tensegrities with an odd number of layers (e.g., $n = 3, 5$) and a large overlap ratio (i.e., for λ close to 1). Since the condition (c) is also necessary, these configurations are not super-stable. For relatively small overlap ratios λ and small per-layer strut numbers m, the tensegrities are guaranteed to be super-stable. By contrast, for prismatic tensegrities with an even number of layers (e.g., $n = 2, 4, 6$), the force density matrix $\mathbf{E}$ is always positive semi-definite under any overlap ratio $\gamma \in (0, 1)$. For relatively small per-layer strut numbers $m = 3, 4, \ldots, 8$, these tensegrities are all super-stable.

When m becomes large (e.g., $m = 30$), super-stability is observed only for small overlap ratios (i.e., λ close to 0). In all cases, a small, positive overlap ratio γ and a small per-layer strut number m tend to promote super-stability in multilayer prismatic tensegrities. An analytical solution to the super-stability conditions for multilayer prismatic tensegrities is beyond the scope of the present work and is left for future study.

Appendix D. Analytical solutions for infinitesimally flexible Kresling origami

In this appendix, we present analytical solutions for the kinematics of the infinitesimally flexible Kresling origami. We first derive closed-form expressions for the nodal displacements of a one-layer Kresling origami and map these infinitesimal displacements to the corresponding dihedral-angle variations. By virtue of the duality theory, these results can be directly translated to characterize the self-equilibrium of the corresponding one-layer prismatic tensegrity.

D.1. Folding kinematics in terms of nodal displacements

As shown in Fig. D.17(a), the configuration of a Kresling origami is determined by the edge number m of each base polygon, twist angle α between the two base polygons, radius r of the circumscribed circle, and height h. We begin by deriving the condition for the existence of infinitesimal mechanisms. As shown in Fig. D.17(b), we examine the folding of the creases incident at node A. Owing to the dihedral symmetry of the Kresling origami, the folding kinematics at all other nodes are identical. We write the position vectors of nodes A, B, C, D, E as

$$\mathbf{r}_A = \begin{bmatrix} r \\ 0 \\ 0 \end{bmatrix}, \quad \mathbf{r}_B = \begin{bmatrix} r\cos(2\pi/m) \\ r\sin(2\pi/m) \\ 0 \end{bmatrix}, \quad \mathbf{r}_C = \begin{bmatrix} r\cos\alpha \\ r\sin\alpha \\ h \end{bmatrix}, \quad \mathbf{r}_D = \begin{bmatrix} r\cos(\alpha+2\pi/m) \\ r\sin(\alpha+2\pi/m) \\ h \end{bmatrix}, \quad \mathbf{r}_E = \begin{bmatrix} r\cos(2\pi/m) \\ -r\sin(2\pi/m) \\ 0 \end{bmatrix}, \tag{D.1}$$

respectively. We denote the displacement of node A by

$$\mathrm{d}\mathbf{r}_A = \begin{bmatrix} \mathrm{d}x \\ \mathrm{d}y \\ \mathrm{d}z \end{bmatrix}. \tag{D.2}$$

The displacements of nodes B, C, D, E can then be expressed as

$$\mathrm{d}\mathbf{r}_B = R_z(2\pi/m)\,\mathrm{d}\mathbf{r}_A, \quad \mathrm{d}\mathbf{r}_C = R_z(\alpha)\,R_x(\pi)\,\mathrm{d}\mathbf{r}_A, \quad \mathrm{d}\mathbf{r}_D = R_z(\alpha+2\pi/m)\,R_x(\pi)\,\mathrm{d}\mathbf{r}_A, \quad \mathrm{d}\mathbf{r}_E = R_z^{\mathrm{T}}(2\pi/m)\,\mathrm{d}\mathbf{r}_A, \tag{D.3}$$

respectively, where the rotation matrices are defined by

$$R_x(t) = \begin{bmatrix} 1 & 0 & 0 \\ 0 & \cos t & -\sin t \\ 0 & \sin t & \cos t \end{bmatrix}, \quad R_z(t) = \begin{bmatrix} \cos t & -\sin t & 0 \\ \sin t & \cos t & 0 \\ 0 & 0 & 1 \end{bmatrix}. \tag{D.4}$$

The creases AB, AC, AD, AE are incident to the node A. We write their direction vectors as

$$\mathbf{r}_{AB} = \begin{bmatrix} r\cos(2\pi/m)-r \\ r\sin(2\pi/m) \\ 0 \end{bmatrix}, \quad \mathbf{r}_{AC} = \begin{bmatrix} r\cos\alpha-r \\ r\sin\alpha \\ h \end{bmatrix}, \quad \mathbf{r}_{AD} = \begin{bmatrix} r\cos(\alpha+2\pi/m)-r \\ r\sin(\alpha+2\pi/m) \\ h \end{bmatrix}, \quad \mathbf{r}_{AE} = \begin{bmatrix} r\cos(2\pi/m)-r \\ -r\sin(2\pi/m) \\ 0 \end{bmatrix}. \tag{D.5}$$

If the displacements $\mathrm{d}\mathbf{r}_I$ $(I = A, B, C, D, E)$ constitute an infinitesimal mechanism of the Kresling origami, they do not alter the corresponding edge lengths. This condition can be formulated as

$$\begin{cases} \mathbf{r}_{AB}\cdot(\mathrm{d}\mathbf{r}_B - \mathrm{d}\mathbf{r}_A) = 0, \\ \mathbf{r}_{AC}\cdot(\mathrm{d}\mathbf{r}_C - \mathrm{d}\mathbf{r}_A) = 0, \\ \mathbf{r}_{AD}\cdot(\mathrm{d}\mathbf{r}_D - \mathrm{d}\mathbf{r}_A) = 0. \end{cases} \tag{D.6}$$

We note that, due to rotational symmetry, the conditions $\mathbf{r}_{AE}\cdot(\mathrm{d}\mathbf{r}_E - \mathrm{d}\mathbf{r}_A) = 0$ and $\mathbf{r}_{AB}\cdot(\mathrm{d}\mathbf{r}_B - \mathrm{d}\mathbf{r}_A) = 0$ are equivalent, and it suffices to consider only one of them. Eq. (D.6) is a linear system with respect to the unknown vector $\mathrm{d}\mathbf{r}_A = [\mathrm{d}x, \mathrm{d}y, \mathrm{d}z]^{\mathrm{T}}$. Collecting the coefficients into a matrix $\mathbf{A}$, we rewrite Eq. (D.6) in compact form as

$$\mathbf{A}\cdot\mathrm{d}\mathbf{r}_A = \begin{bmatrix} 4r\sin^2(\pi/m) & 0 & 0 \\ 2r-2r\cos\alpha & -2r\sin\alpha & -2\,h \\ 2r-2r\cos(\alpha+2\pi/m) & -2r\sin(\alpha+2\pi/m) & -2\,h \end{bmatrix} \begin{bmatrix} \mathrm{d}x \\ \mathrm{d}y \\ \mathrm{d}z \end{bmatrix} = \begin{bmatrix} 0 \\ 0 \\ 0 \end{bmatrix}. \tag{D.7}$$

For nonzero solutions to exist, the matrix $\mathbf{A}$ must be singular; that is,

$$\boxed{\det(\mathbf{A}) = -32\,hr^2\sin^3\left(\frac{\pi}{m}\right)\cos\left(\alpha+\frac{\pi}{m}\right) = 0.} \tag{D.8}$$

By solving Eq. (D.8), we obtain

$$\boxed{\alpha = \frac{\pi}{2} - \frac{\pi}{m}.} \tag{D.9}$$

This condition represents the compatibility requirement for the Kresling origami to admit infinitesimal mechanisms. *As a consequence of the duality, it takes exactly the same form as the self-equilibrium condition for a one-layer prismatic tensegrity given in Eq. (C.1)*. Under the condition given in Eq. (D.9), solving Eq. (D.7) yields

$$\boxed{\mathrm{d}x = 0, \quad \mathrm{d}y = -\frac{h\sec(\pi/m)}{r}\mathrm{d}z.} \tag{D.10}$$

The displacements of nodes A, B, C, D, and E can therefore be written as

$$\begin{aligned}
&\mathrm{d}\mathbf{r}_A = \mathrm{d}z\begin{bmatrix} 0 \\ -(h/r)\sec(\pi/m) \\ 1 \end{bmatrix}, \quad \mathrm{d}\mathbf{r}_B = \mathrm{d}z\begin{bmatrix} 2(h/r)\sin(\pi/m) \\ -(h/r)\sec(\pi/m)\cos(2\pi/m) \\ 1 \end{bmatrix}, \\
&\mathrm{d}\mathbf{r}_C = \mathrm{d}z\begin{bmatrix} -h/r \\ (h/r)\tan(\pi/m) \\ -1 \end{bmatrix}, \quad \mathrm{d}\mathbf{r}_D = \mathrm{d}z\begin{bmatrix} -h/r \\ -(h/r)\tan(\pi/m) \\ -1 \end{bmatrix}, \quad \mathrm{d}\mathbf{r}_E = \mathrm{d}z\begin{bmatrix} -2(h/r)\sin(\pi/m) \\ -(h/r)\sec(\pi/m)\cos(2\pi/m) \\ 1 \end{bmatrix},
\end{aligned} \tag{D.11}$$

respectively. The vertical displacement component $\mathrm{d}z$ serves as a free parameter that scales the magnitude of the deformation. To describe the locations and displacements of all nodes, we label the bottom nodes by indices $1, 2, \ldots, m$ and the top nodes by $m+1, m+2, \ldots, 2m$, as illustrated in Fig. D.17(a). Under this indexing scheme, the coordinates of each node i can be expressed as

$$\mathbf{r}_i = \begin{cases} R_z[2(i-1)\pi/m]\ \mathbf{r}_1, & i = 1, 2, \ldots, m, \\ R_z[2(i-m-1)\pi/m]\ \mathbf{r}_{m+1}, & i = m+1, m+2, \ldots, 2m. \end{cases} \tag{D.12}$$

The corresponding displacement can be expressed as

$$\mathrm{d}\mathbf{r}_i = \begin{cases} R_z[2(i-1)\pi/m]\ \mathrm{d}\mathbf{r}_1, & i = 1, 2, \ldots, m, \\ R_z[2(i-m-1)\pi/m]\ \mathrm{d}\mathbf{r}_{m+1}, & i = m+1, m+2, \ldots, 2m. \end{cases} \tag{D.13}$$

Specifically, the coordinates and displacements of nodes A, B, C, D, E correspond to those indexed by 1, 2, $m+1$, $m+2$, m, respectively. That is, $\mathbf{r}_1 = \mathbf{r}_A$, $\mathbf{r}_2 = \mathbf{r}_B$, $\mathbf{r}_{m+1} = \mathbf{r}_C$, $\mathbf{r}_{m+2} = \mathbf{r}_D$, $\mathbf{r}_m = \mathbf{r}_E$, $\mathrm{d}\mathbf{r}_1 = \mathrm{d}\mathbf{r}_A$, $\mathrm{d}\mathbf{r}_2 = \mathrm{d}\mathbf{r}_B$, $\mathrm{d}\mathbf{r}_{m+1} = \mathrm{d}\mathbf{r}_C$, $\mathrm{d}\mathbf{r}_{m+2} = \mathrm{d}\mathbf{r}_D$, $\mathrm{d}\mathbf{r}_m = \mathrm{d}\mathbf{r}_E$. Since these coordinates and displacements have been derived, Eq. (D.12) can be written in component form as

$$\boxed{\mathbf{r}_i = \begin{cases} \begin{bmatrix} r\cos[(2i-2)\pi/m] \\ r\sin[(2i-2)\pi/m] \\ 0 \end{bmatrix}, & i = 1, 2, \ldots, m, \\ \begin{bmatrix} r\sin[(3-2i+2m)\pi/m] \\ r\cos[(3-2i+2m)\pi/m] \\ h \end{bmatrix}, & i = m+1, m+2, \ldots, 2m. \end{cases}} \tag{D.14}$$

Similarly, Eq. (D.13) can be written as

$$\boxed{\mathrm{d}\mathbf{r}_i = \begin{cases} \mathrm{d}z\begin{bmatrix} (h/r)\sec(\pi/m)\sin[(2i-2)\pi/m] \\ -(h/r)\sec(\pi/m)\cos[(2i-2)\pi/m] \\ 1 \end{bmatrix}, & i = 1, 2, \ldots, m, \\ \mathrm{d}z\begin{bmatrix} -(h/r)\sec(\pi/m)\cos[(3-2i+2m)\pi/m] \\ (h/r)\sec(\pi/m)\sin[(3-2i+2m)\pi/m] \\ -1 \end{bmatrix}, & i = m+1, m+2, \ldots, 2m. \end{cases}} \tag{D.15}$$

D.2. Folding kinematics in terms of dihedral-angle variations

To relate the nodal displacements to the variations of the dihedral angles, we adopt the Jacobian formulation proposed by Liu and Paulino (2017):

$$\begin{aligned}
\frac{\partial\theta}{\partial\mathbf{r}_{\hat{i}}} &= \frac{\|\mathbf{r}_{\hat{k}\hat{j}}\|}{\|\mathbf{N}_{\hat{i}}\|^2}\mathbf{N}_{\hat{i}}, \\
\frac{\partial\theta}{\partial\mathbf{r}_{\hat{\ell}}} &= -\frac{\|\mathbf{r}_{\hat{k}\hat{j}}\|}{\|\mathbf{N}_{\hat{\ell}}\|^2}\mathbf{N}_{\hat{\ell}}, \\
\frac{\partial\theta}{\partial\mathbf{r}_{\hat{j}}} &= \left(\frac{\mathbf{r}_{\hat{i}\hat{j}}\cdot\mathbf{r}_{\hat{k}\hat{j}}}{\|\mathbf{r}_{\hat{k}\hat{j}}\|^2} - 1\right)\frac{\partial\theta}{\partial\mathbf{r}_{\hat{i}}} - \frac{\mathbf{r}_{\hat{k}\hat{\ell}}\cdot\mathbf{r}_{\hat{k}\hat{j}}}{\|\mathbf{r}_{\hat{k}\hat{j}}\|^2}\frac{\partial\theta}{\partial\mathbf{r}_{\hat{\ell}}}, \\
\frac{\partial\theta}{\partial\mathbf{r}_{\hat{k}}} &= \left(\frac{\mathbf{r}_{\hat{k}\hat{\ell}}\cdot\mathbf{r}_{\hat{k}\hat{j}}}{\|\mathbf{r}_{\hat{k}\hat{j}}\|^2} - 1\right)\frac{\partial\theta}{\partial\mathbf{r}_{\hat{\ell}}} - \frac{\mathbf{r}_{\hat{i}\hat{j}}\cdot\mathbf{r}_{\hat{k}\hat{j}}}{\|\mathbf{r}_{\hat{k}\hat{j}}\|^2}\frac{\partial\theta}{\partial\mathbf{r}_{\hat{i}}},
\end{aligned} \tag{D.16}$$

where $\mathbf{r}_{\hat{i}\hat{j}} = \mathbf{r}_{\hat{i}} - \mathbf{r}_{\hat{j}}$, $\mathbf{r}_{\hat{k}\hat{j}} = \mathbf{r}_{\hat{k}} - \mathbf{r}_{\hat{j}}$, $\mathbf{r}_{\hat{k}\hat{\ell}} = \mathbf{r}_{\hat{k}} - \mathbf{r}_{\hat{\ell}}$, $\mathbf{N}_{\hat{i}} = \mathbf{r}_{\hat{i}\hat{j}} \times \mathbf{r}_{\hat{k}\hat{j}}$, $\mathbf{N}_{\hat{\ell}} = \mathbf{r}_{\hat{k}\hat{j}} \times \mathbf{r}_{\hat{k}\hat{\ell}}$. As illustrated in the bottom inset of Fig. D.17(b), the dihedral angle θ is defined by nodes $\hat{j}$ and $\hat{k}$ on the corresponding crease, and by nodes $\hat{i}$ and $\hat{\ell}$ that specify the two adjacent panels. Specifically, we consider the dihedral angles θ_{AB}, θ_{AC}, θ_{AD}, whose infinitesimal variations are expressed as

$$\begin{aligned}
\mathrm{d}\theta_{AB} &= \frac{\partial \theta_{AB}}{\partial \mathbf{r}_D} \cdot \mathrm{d}\mathbf{r}_D + \frac{\partial \theta_{AB}}{\partial \mathbf{r}_E} \cdot \mathrm{d}\mathbf{r}_E + \frac{\partial \theta_{AB}}{\partial \mathbf{r}_A} \cdot \mathrm{d}\mathbf{r}_A + \frac{\partial \theta_{AB}}{\partial \mathbf{r}_B} \cdot \mathrm{d}\mathbf{r}_B, \\
\mathrm{d}\theta_{AC} &= \frac{\partial \theta_{AC}}{\partial \mathbf{r}_E} \cdot \mathrm{d}\mathbf{r}_E + \frac{\partial \theta_{AC}}{\partial \mathbf{r}_D} \cdot \mathrm{d}\mathbf{r}_D + \frac{\partial \theta_{AC}}{\partial \mathbf{r}_A} \cdot \mathrm{d}\mathbf{r}_A + \frac{\partial \theta_{AC}}{\partial \mathbf{r}_C} \cdot \mathrm{d}\mathbf{r}_C, \\
\mathrm{d}\theta_{AD} &= \frac{\partial \theta_{AD}}{\partial \mathbf{r}_C} \cdot \mathrm{d}\mathbf{r}_C + \frac{\partial \theta_{AD}}{\partial \mathbf{r}_B} \cdot \mathrm{d}\mathbf{r}_B + \frac{\partial \theta_{AD}}{\partial \mathbf{r}_A} \cdot \mathrm{d}\mathbf{r}_A + \frac{\partial \theta_{AD}}{\partial \mathbf{r}_D} \cdot \mathrm{d}\mathbf{r}_D.
\end{aligned} \tag{D.17}$$

By applying Eqs. (D.14) and (D.16), we simplify Eq. (D.17) into

$$\frac{\mathrm{d}\theta_{AB}}{\|\mathbf{r}_{AB}\|} = \frac{2\mathrm{d}z}{r^2 \sin(2\pi/m)}, \quad \frac{\mathrm{d}\theta_{AC}}{\|\mathbf{r}_{AC}\|} = \frac{2\mathrm{d}z}{r^2 \cos(\pi/m)}, \quad \frac{\mathrm{d}\theta_{AD}}{\|\mathbf{r}_{AD}\|} = -\frac{2\mathrm{d}z}{r^2 \cos(\pi/m)}. \tag{D.18}$$

The free parameter $\mathrm{d}z$ scales the magnitude of the folding, consistent with the displacement formulation given in Eq. (D.11) or (D.15). Considering the dihedral symmetry, the folding angle per unit crease ij can be expressed as

$$\boxed{\frac{\mathrm{d}\theta_{ij}}{\|\mathbf{r}_{ij}\|} = \begin{cases} \dfrac{2\mathrm{d}z}{r^2 \sin(2\pi/m)}, & j = i+1, \quad i = 1, 2, \ldots, 2m \\ \dfrac{2\mathrm{d}z}{r^2 \cos(\pi/m)}, & j = i+m, \quad i = 1, 2, \ldots, m \\ -\dfrac{2\mathrm{d}z}{r^2 \cos(\pi/m)}, & j = i+m+1, \quad i = 1, 2, \ldots, m, \end{cases}} \tag{D.19}$$

where $j = i+1$ cycles to $j = 1$ for $i = m$ and to $j = m+1$ for $i = 2m$; $j = i+m+1$ cycles to $j = m+1$ for $i = m$. It is noteworthy that Eq. (D.18) can be rewritten as

$$\boxed{\begin{array}{l} \dfrac{\mathrm{d}\theta_{AB}/\|\mathbf{r}_{AB}\|}{-\mathrm{d}\theta_{AD}/\|\mathbf{r}_{AD}\|} = \dfrac{1}{2\sin\frac{\pi}{m}}, \\ \dfrac{\mathrm{d}\theta_{AC}/\|\mathbf{r}_{AC}\|}{-\mathrm{d}\theta_{AD}/\|\mathbf{r}_{AD}\|} = 1. \end{array}} \tag{D.20}$$

Eq. (D.20) takes exactly the same form as the force densities for a one-layer prismatic tensegrity given in Eq. (C.2), indicating the equivalence between force densities and infinitesimal folding angles per unit crease length under the duality relationship. Moreover, taking Eqs. (D.14) and (D.19), one can verify the following folding compatibility

$$\mathrm{d}\theta_{AB} \frac{\mathbf{r}_{AB}}{\|\mathbf{r}_{AB}\|} + \mathrm{d}\theta_{AC} \frac{\mathbf{r}_{AC}}{\|\mathbf{r}_{AC}\|} + \mathrm{d}\theta_{AD} \frac{\mathbf{r}_{AD}}{\|\mathbf{r}_{AD}\|} + \mathrm{d}\theta_{AE} \frac{\mathbf{r}_{AE}}{\|\mathbf{r}_{AE}\|} = \mathbf{0}, \tag{D.21}$$

which implies that all panels incident to a given node preserve their connectivity during the infinitesimal folding. Eq. (D.21) takes exactly the same form as the nodal force balance condition for a one-layer prismatic tensegrity, as illustrated in the middle inset of Fig. D.17. Denoting the member forces by F_{AB}, F_{AC}, F_{AD}, F_{AE}, the equilibrium equation can be written as

$$F_{AB} \frac{\mathbf{r}_{AB}}{\|\mathbf{r}_{AB}\|} + F_{AC} \frac{\mathbf{r}_{AC}}{\|\mathbf{r}_{AC}\|} + F_{AD} \frac{\mathbf{r}_{AD}}{\|\mathbf{r}_{AD}\|} + F_{AE} \frac{\mathbf{r}_{AE}}{\|\mathbf{r}_{AE}\|} = \mathbf{0}. \tag{D.22}$$

Eqs. (D.21) and (D.22) capture the duality between origami and tensegrity in terms of folding angles and internal forces. More generally, this relationship can be written as

$$\boxed{\frac{\mathrm{d}\theta_{ij,p}}{\mathrm{d}\theta_{k\ell,p}} = \frac{F_{ij,p}}{F_{k\ell,p}},} \tag{D.23}$$

where ij and $k\ell$ denote two members of the tensegrity, or equivalently, two creases of the origami. Eq. (D.23) characterizes the p-th branch of the independent states of self-stress of the tensegrity or, equivalently, the p-th independent infinitesimal mechanism of the origami. For the Kresling origami and the one-layer prismatic tensegrity, there exists only a single branch (Fig. 6(a)). In contrast, for stacked origami towers and class-2 tensegrity towers (Fig. 6(b)–(d)), there are n distinct branches, indexed by $p = 1, 2, \ldots, n$, where n denotes the number of layers.

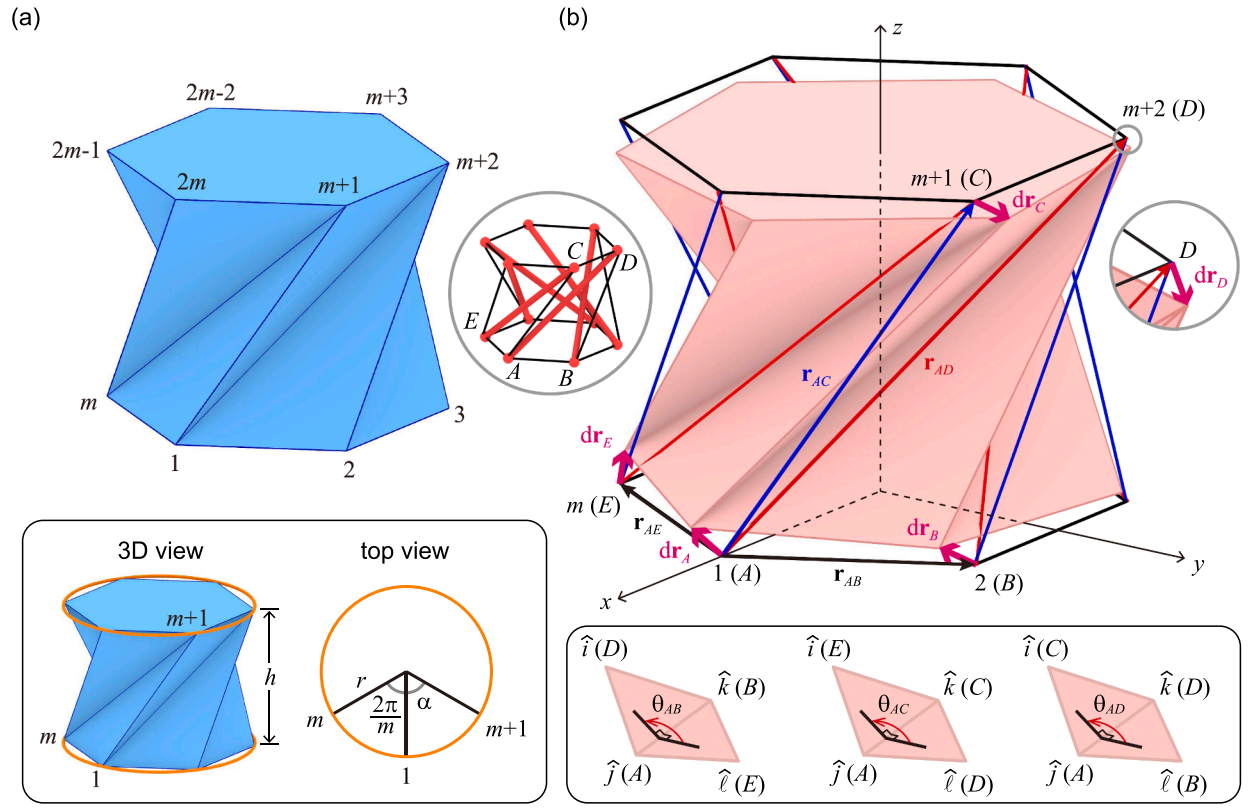

Fig. D.17. Shaky Kresling origami. (a) Configuration with hexagonal base polygons. In general, for base polygons with m sides, the corresponding twist angle is given by $\alpha = \pi/2 - \pi/m$. (b) The infinitesimal mechanisms with representative nodal displacements $\mathrm{d}\mathbf{r}_A$, $\mathrm{d}\mathbf{r}_B$, $\mathrm{d}\mathbf{r}_C$, $\mathrm{d}\mathbf{r}_D$, $\mathrm{d}\mathbf{r}_E$. The bottom inset shows the dihedral angles θ_{AB}, θ_{AC}, θ_{AD}. The left inset shows a dual tensegrity.

Appendix E. Particular case of duality in two dimensions

The duality of tensegrity and origami can also be applied to two-dimensional configurations. An example is the cross-X tensegrity and the collapsed tetrahedron, as shown in Fig. E.18. The X-cross tensegrity is self-balanced, with the struts and cables carrying internal forces $-\sqrt{2}T$ and T, respectively (Zhang and Ohsaki, 2015). This state of self-stress is dual to the infinitesimal mechanism of

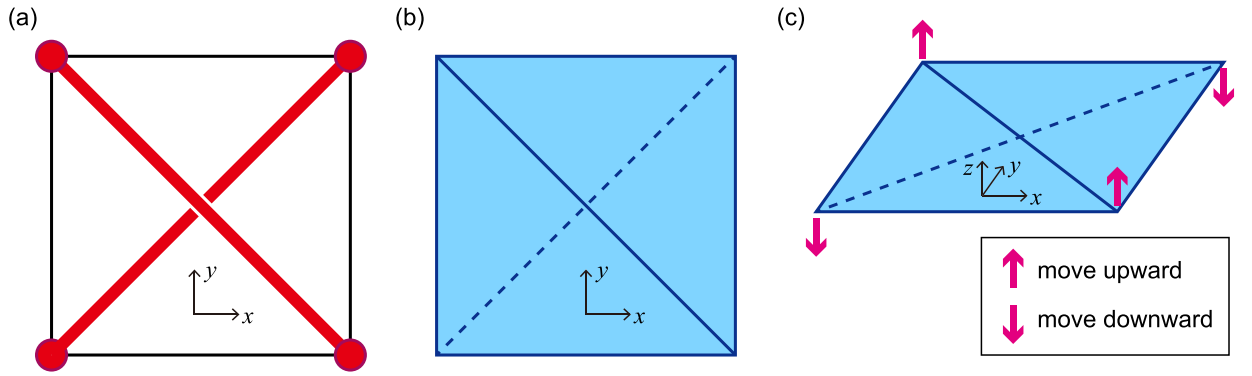

Fig. E.18. Two-dimensional dual configurations of tensegrity and origami. (a) The two-dimensional X-cross tensegrity, composed of four cables, shown as thin black segments, and two struts, shown as thick red segments. Ideally, the struts do not physically contact each other at the center. (b) The two-dimensional origami in the form of a collapsed tetrahedron, composed of four faces that are identical right triangles. (c) The infinitesimal mechanism of the collapsed tetrahedron, in which one diagonal moves upward while the other moves downward. This mechanism is dual to the state of self-stress of the X-cross tensegrity.

the collapsed tetrahedron, in which one diagonal moves upward while the other moves downward. This duality can be readily verified by prescribing the magnitude of nodal displacements u and the square side length L, which gives the infinitesimal dihedral-angle variations $-2u/(L/\sqrt{2}) = -2\sqrt{2}u/L$ at each diagonal and $2u/L$ at each square edge.

References

Aigner, M., Ziegler, G.M., 2010. Cauchy's rigidity theorem, Proofs from THE BOOK. Springer, Berlin, Heidelberg. pp. 81–84.
Alexandrov, A.D., 1950. Infinitesimal rigidity of convex polyhedra with stationary development, Convex Polyhedra. Gosudarstv. Izdat. Tekhn.-Teor. Lit., Moscow-Leningrad. English translation: Springer Berlin, Heidelberg, 2005.
Asimow, L., Roth, B., 1978. The rigidity of graphs. Trans. Am. Math. Soc. 245, 279–289.
Asimow, L., Roth, B., 1979. The rigidity of graphs, II. J. Math. Anal. Appl. 68 (1), 171–190.
Bansod, Y.D., Nandanwar, D., Burša, J., 2014. Overview of tensegrity-I: Basic structures. Eng. Mechan. 21, 355–367.
Blaschke, W., 1920. Über affine geometrie XXVI: Wackelige achtflache. Math. Z. 6 (1), 85–93.
Bricard, R., 1897. Mémoire sur la théorie de l'octaèdre articulé. J. Mathémat. Pure. Appliqué. 3, 113–148. English translation: E. A. Coutsias, 2010. Memoir on the theory of the articulated octahedron. arXiv:1203.1286.
Cauchy, A., 1813. Deuxieme memoire sur les polygones et les polydres. J. l'école Polytech. XVIeme cahier, 87–98.
Cera, A. B.M., 2020. Design, Control, and Motion Planning of Cable-Driven Flexible Tensegrity Robots. Ph.D. thesis. UC Berkeley.
Chen, B. G.-g., Santangelo, C.D., 2018. Branches of triangulated origami near the unfolded state. Phys. Rev. X 8 (1), 011034.
Connelly, R., 1976. An immersed polyhedral surface which flexes. Ind. Univ. Math. J. 25 (10), 965–972.
Connelly, R., 1977. A counterexample to the rigidity conjecture for polyhedra. Publications Mathématiques de l'IHÉS 47, 333–338.
Connelly, R., 1978. A flexible sphere. Math. Intell. 1 (3), 130–131.
Connelly, R., 1979. The rigidity of polyhedral surfaces. Math. Mag. 52 (5), 275–283.
Connelly, R., 1980. The rigidity of certain cabled frameworks and the second-order rigidity of arbitrarily triangulated convex surfaces. Adv. Math. 37 (3), 272–299.
Connelly, R., 2002. Tensegrity Structures: Why are they Stable? Springer US, Boston, MA. pp. 47–54.
Connelly, R., Terrell, M., 1995. Globally Rigid Symmetric Tensegrities. Structural Topology 21, 59-79.
Connelly, R., Whiteley, W., 1996. Second-order rigidity and prestress stability for tensegrity frameworks. SIAM J. Discret. Math. 9 (3), 453–491.
Crapo, H., Whiteley, W., 1982. Statics of frameworks and motions of panel structures: a projective geometric introduction. Structural Topology 6, 43–82.
Cromwell, P.R., 1997. Equality, rigidity and flexibility, Polyhedra: "One of the Most Charming Chapters of Geometry". Cambridge University Press, Cambridge, UK. pp. 219–248.
Dang, X., Paulino, G.H., 2026. Invariant dual mechanics of tensegrity and origami. Proc. Natl. Acad. Sci. 123 (12), e2519138123.
Dehn, M., 1916. Über die starrheit konvexer polyeder. Math. Ann. 77 (4), 466–473.
Demaine, E.D., O'Rourke, J., 2007a. Flexible polyhedra, Geometric Folding Algorithms: Linkages, Origami, Polyhedra. Cambridge University Press, New York, NY. pp. 345–348.
Demaine, E.D., O'Rourke, J., 2007b. Tensegrities, Geometric Folding Algorithms: Linkages, Origami, Polyhedra. Cambridge University Press, New York, NY. pp. 53–57.
Fraternali, F., Rimoli, J.J., 2025. Tensegrity Systems: Basic Concepts, Mechanical Metamaterials, Biotensegrity. Springer.
Gan, B.S., 2020. Computational Modeling of Tensegrity Structures. Springer.
Gluck, H., 1975. Almost all simply connected closed surfaces are rigid. In: Glaser, L.C., Rushing, T.B. (Eds.), Geometric Topology. Springer, Berlin, Heidelberg, pp. 225–239.
Goldberg, M., 1978. Unstable polyhedral structures. Math. Mag. 51 (3), 165–170.
Guest, S.D., Hutchinson, J.W., 2003. On the determinacy of repetitive structures. J. Mech. Phys. Solids 51 (3), 383–391.
Jessen, B., 1967. Orthogonal icosahedra. Nord. Mat. Tidskr., 90–96.
Kresling, B., 2008. Natural twist buckling in shells: From the hawkmoth's bellows to the deployable Kresling-pattern and cylindrical Miura-ori. In: Proceedings of the 6th International Conference on Computation of Shell and Spatial Structures. Vol. 11. International Association for Shell and Spatial Structures, Ithaca, NY, pp. 12–32.
Li, J., 2018. Flexible Polyhedra - Exploring Finite Mechanisms of Triangulated Polyhedra. Ph.D. thesis. University of Cambridge.
Liu, K., Paulino, G.H., 2017. Nonlinear mechanics of non-rigid origami: An efficient computational approach. Proc. R. Soc. A 473 (2206), 20170348.
Lu, L., Dang, X., Feng, F., Lv, P., Duan, H., 2022. Conical Kresling origami and its applications to curvature and energy programming. Proc. R. Soc. A 478 (2257), 20210712.
Maksimov, I.G., 1995. Polyhedra with bendings and Riemann surfaces. Russ. Math. Surv. 50 (4), 821.
Maxwell, J.C., 1864. On the calculation of the equilibrium and stiffness of frames. Lond. Edinb. Dublin Philos. Mag. J. Sci. 27 (182), 294–299.
McInerney, J., Chen, B. G.-g., Theran, L., Santangelo, C.D., Rocklin, D.Z., 2020. Hidden symmetries generate rigid folding mechanisms in periodic origami. Proc. Natl. Acad. Sci. 117 (48), 30252–30259.
Misseroni, D., Pratapa, P.P., Liu, K., Kresling, B., Chen, Y., Daraio, C., Paulino, G.H., 2024. Origami engineering. Nature Reviews Methods Primers 4 (1), 40.
Nishimura, Y., 2000. Static and Dynamic Analyses of Tensegrity Structures. Ph.D. thesis. University of California, San Diego, USA.
Pellegrino, S., Calladine, C.R., 1986. Matrix analysis of statically and kinematically indeterminate frameworks. Int. J. Solids Struct. 22 (4), 409–428.
Roth, B., Whiteley, W., 1981. Tensegrity frameworks. Trans. Am. Math. Soc. 265 (2), 419–446.
Schönhardt, E., 1928. Über die zerlegung von dreieckspolyedern in tetraeder. Math. Ann. 98, 309–312.
Servatius, B., 2018. Polyhedra in 3-space. In: Sitharam, M., Audrey St. John, J.S. (Ed.), Handbook of Geometric Constraint Systems Principles. CRC Press, Boca Raton, FL, pp. 289–298.
Skelton, R.E., de Oliveira, M.C., 2009. Tensegrity Systems. Springer.
Snelson, K.D., 1965. Continuous tension, discontinuous compression structures. US Patent 3169611.
Sultan, C., 1999. Modeling, Design, and Control of Tensegrity Structures with Applications. Ph.D. thesis. Purdue University.
Tachi, T., 2009. Simulation of rigid origami. In: Origami 4: Fourth International Meeting on Origami in Science, Mathematics and Education, pp. 175–187.
Tachi, T., 2012. Design of infinitesimally and finitely flexible origami based on reciprocal figures. J. Geom. Graph. 16 (2), 223–234.
Tachi, T., 2015. Rigid folding of periodic origami tessellations. In: Origami 6: Sixth International Meeting on Origami in Science, Mathematics and Education, pp. 97–108.
Tibert, G., 2002. Deployable Tensegrity Structures for Space Applications. Ph.D. thesis. KTH Royal Institute of Technology, Stockholm, Sweden.
Wells, D., 1997. The Penguin Dictionary of Curious and Interesting Geometry. Penguin Group, London. pp. 161–162.
Wunderlich, W., 1986. Eine familie von geschlossenen gleichflächigen polyedern, die fast beweglich sind. Elem. Math. 41, 88–98.
Zang, S., Misseroni, D., Zhao, T., Paulino, G.H., 2024. Kresling origami mechanics explained: Experiments and theory. J. Mech. Phys. Solids 188, 105630.
Zhang, J., Ohsaki, M., 2015. Tensegrity Structures: Form, Stability, and Symmetry. Springer, Tokyo.
Zhang, J.Y., Guest, S.D., Ohsaki, M., 2009a. Symmetric prismatic tensegrity structures: Part I. configuration and stability. Int. J. Solids Struct. 46 (1), 1–14.
Zhang, J.Y., Guest, S.D., Ohsaki, M., 2009b. Symmetric prismatic tensegrity structures: Part II. symmetry-adapted formulations. Int. J. Solids Struct. 46 (1), 15–30.
Zhang, L.-Y., Li, Y., Cao, Y.-P., Feng, X.-Q., 2013. A unified solution for self-equilibrium and super-stability of rhombic truncated regular polyhedral tensegrities. Int. J. Solids Struct. 50 (1), 234–245.